Chapter 6

Study of Ti addition on the microstructure, phase equilibria and oxidation behaviour of two Cr-Si based intermetallic alloys

6.1. Introduction

To date, there have been some studies of phase equilibria in the Cr-Si-Al and Cr-Si-Ti systems [10,13,14,40,44,45]. As we have already discussed in chapter 2, Yu et al. [40] studied the Cr-Si-Al ternary system using the CALPHAD method. Gupta [10] presented isothermal sections at 800, 900, 1000 and 1100 ^{o} C of the same system using diffusion couple. Du and Schuster [21], Povarova et al. [133] and Raghavan and Hayes [134,135] obtained experimental data to support a thermodynamic model of the Cr and Ti rich ends of the Cr-Ti-Si system. There is no published data on the phase equilibria of the Cr-Si-Al-Ti quaternary system. In this chapter the microstructure and oxidation of the Cr-45Si-5Al-5Ti (AN3) and Cr-25Si-25Al-5Ti (AN4) alloys (at%) is studied. We are interested in Ti as an alloying addition in Cr-Si-Al as it is expected that Ti from the substrate alloy will diffuse into Cr-Si-Al based bond coat.

6.2. Results

6.2.1 The microstructures of the alloys

The phases present in the alloys were 6-5 and 5-3 silicides, disilicide, Cr aluminides and 3-1 silicide.In this chapter, the Cr_5Si_3 and Ti_5Si_3 5-3 silicides with Ti , Cr and Si in solid solution will be referred to as $(Cr,Ti)_5(Si,Al)_3$ and $(Ti,Cr)_5(Si,Al)_3$, and the $CrSi_2$ desilicide with Al in solid solution as $Cr(Si,Al)_2$. The Ti_6Si_5 silicide with Al and Cr in solid solution will be referred to as $(Ti,Cr)_6(Si,Al)_5$. Likewise, the Cr_5Al_8, Cr_4Al_9 aluminides with Si in solid solution and Cr_3Si with Al in solid solution will be referred to as $Cr_5(Al,Si)_8$, $Cr_4(Al,Si)_9$, $Cr_4(Al,Si)_{11}$ and $Cr_3(Si,Al)$, respectively.

6.2.1.1 As cast Cr-45Si-5Al-5Ti (alloy AN3-AC)

The volume fractions of the phases present in the button ingot of the alloy AN3-AC are given in Table 6-1. The microstructure of AN3-AC consisted of 38.2% Ti_6Si_5, 32.6% $CrSi_2$ and 29.2 % Cr_5Si_3. The data in Table 6-2 summarizes the compositions of the phases in the bulk (centre) of the button. Compared with the nominal composition, the AN3-AC was poorer in Al and richer in Ti.

According to the XRD and EDX data (Figure 6.1 and Table 6-2), the $(Ti,Cr)_6Si_5$, $Cr_5(Si,Al)_3$ and Cr $(Si,Al)_2$ phases were present in AN3-AC (see also Figure 6.2). In the microstructure of the AN3-AC (Figure 6.2 a, b), the of columnar Ti_6Si_5 and Cr_5Si_3 silicides were parallel to each other and the Cr_5Si_3 was formed either adjacent to the 6-5 silicide or was surrounded by $CrSi_2$. In the Ti_6Si_5 silicide, there was no solubility of Al and the maximum solubility of Ti was 12.0 at.%. In the Cr_5Si_3, the Ti and Al solubilities were low. In the $CrSi_2$ there was no solubility of Ti and 15 at.% Si was substituted by Al.

6.2.1.2 Heat treated Cr-45Si-5Al-5Ti (alloy AN3-HT)

The alloy was given two different heat treatments, namely 1200 ^{o}C /100 h and 1300 ^{o}C/100h. The actual composition of the heat-treated specimen at 1200 ^{o}C was Cr-45.4Si-4.9Ti-5.2Al very close to the nominal composition. According to the XRD data (Figure 6.1) and the chemical

Table 6-1 data for density and % areas of constituent phases in the as cast (AC) and heat treated (HT) alloys AN3 and AN4.

Alloy[a]	**Density (g/cm^3)**	**Ti_6Si_5 (%)**	**Cr_5Si_3 /Ti_5Si_3/ Ti-rich Cr_5Si_3 (%)**	**$CrSi_2$ (%)**	**CrSi /Cr_3Si (%)**	**Al_8Cr_5 (%)**	**Al_9Cr_4 /$Al_{11}Cr_4$ (%)**
AN3-AC	4.89±0.01	38.2	29.2/0/0	32.6	-	-	-
AN3-HT1200	-	46.9	25.6/0/0	27.5	-	-	-
AN3-HT1300	-	43.2	24.4/0/0	25.5	6.9/0	-	-
AN4-AC	4.86±0.01	27.6	7.3/0/22.7	-	-	36.7	5.7/0
AN4-HT1200	-	11.7	42.1/3.3/0	-	0/3.1	39.8	-
AN4-HT1300	-	3.9	1.2/53.7/0	-	0/4.9	32.5	0/3.8

[a] AC=as cast , HT1200 = heat treatment at 1200 °C/100 h, HT1300 = heat treatment at 1300 °C /100 h.

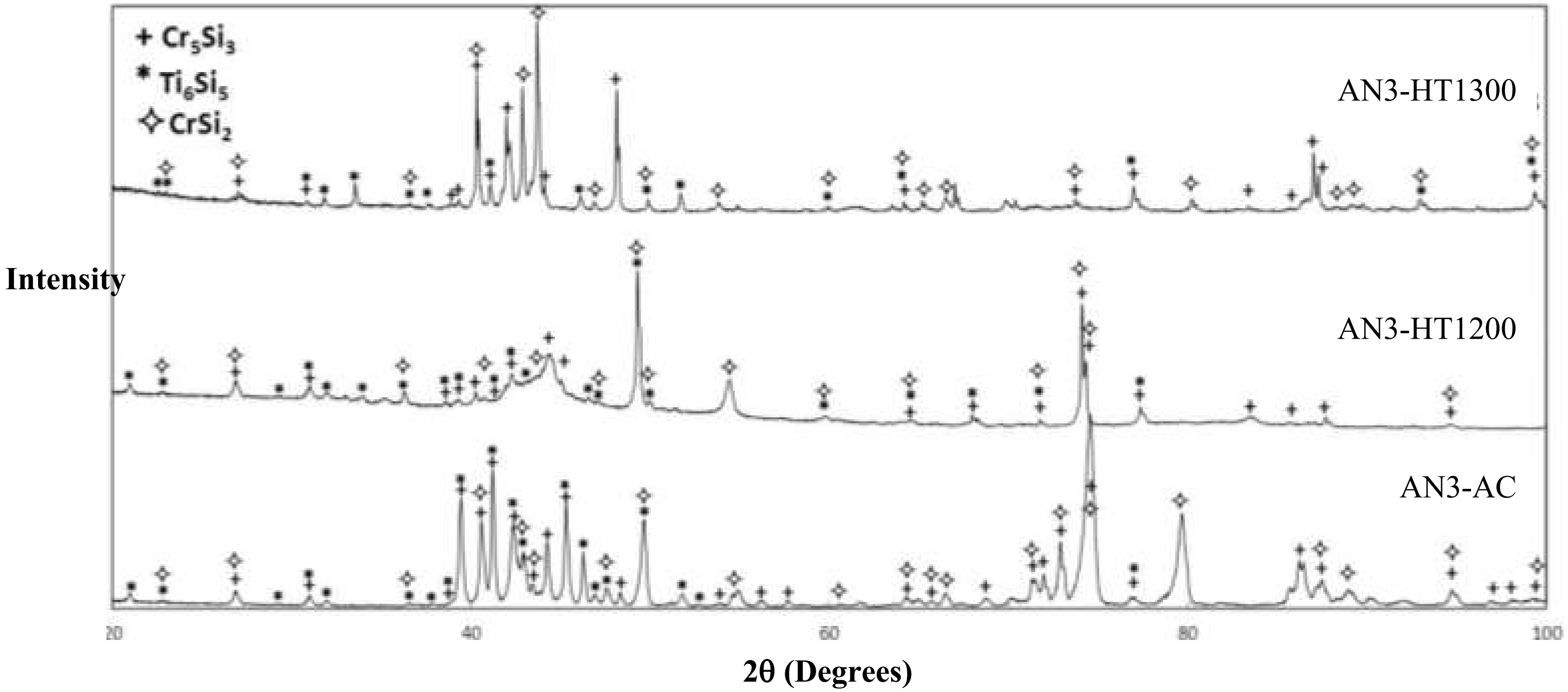

Figure 6.1 X-ray diffractograms of the as cast and heat treated alloy AN3 (card number: 01-089-4866 for $CrSi_2$, 00-050-1329 for Cr_5Si_3 and 04-007-8926 for Ti_6Si_5) (HT1200 = heat treatment at 1200 °C/100 h, HT1300 = heat treatment at 1300 °C /100 h)

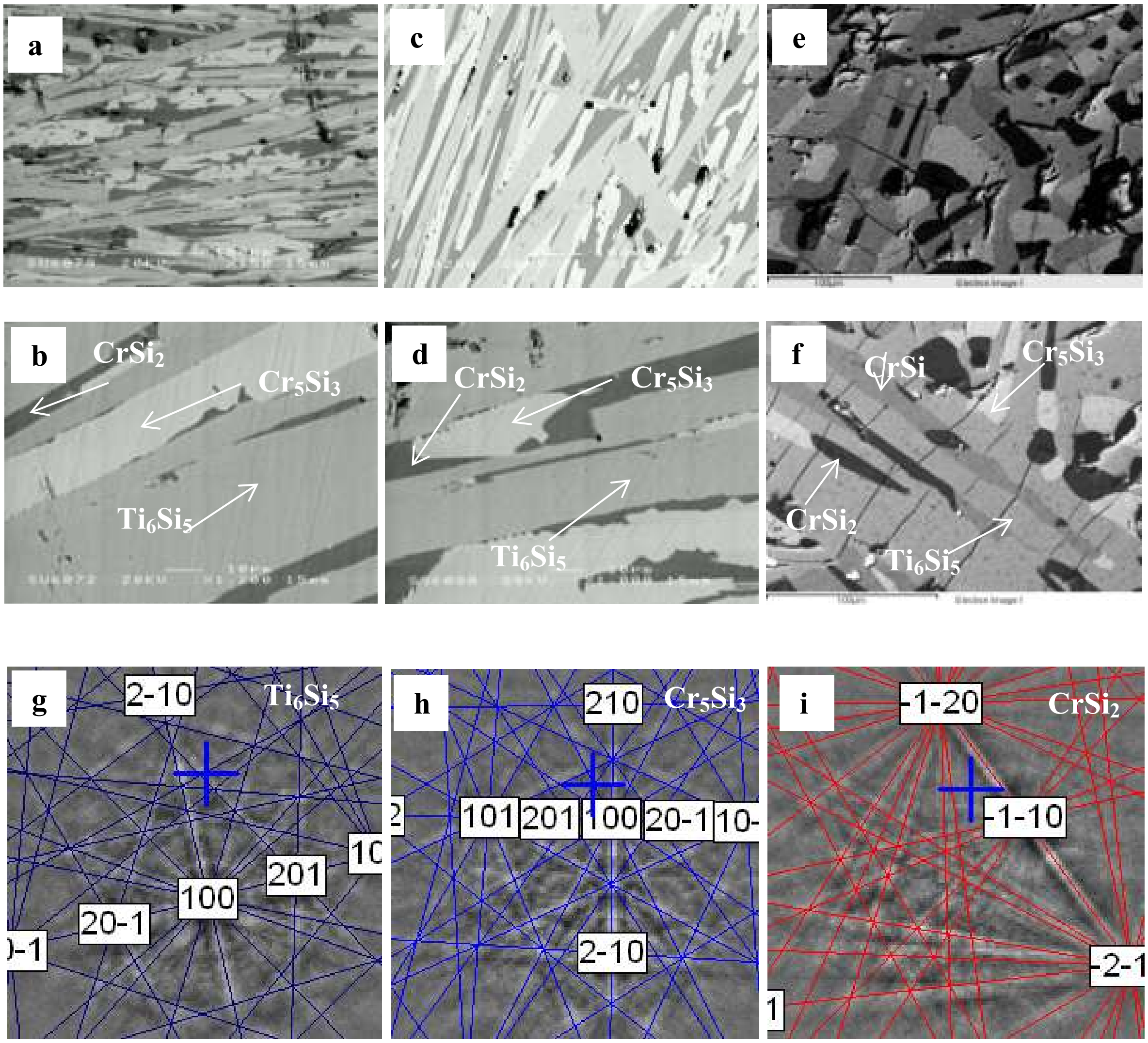

Figure 6.2 Microstructure of alloy AN3 a, b) as-cast c, d) heat-treated at 1200 ° C for 100 h and e, f) heat-treated at 1300 ° C for 100 h and g, h, i) EBSD patterns of Ti_6Si_5, Cr_5Si_3 and $CrSi_2$, respectively.

analysis data (Table 6-2) the heat treated microstructure was stable at 1200 °C and consisted of the same phase, as the AN3-AC namely the Ti_6Si_5, Cr_5Si_3 and $CrSi_2$ silicides. Typical backscatter electron images of AN3-HT1200 are shown in Figure 6.2 (c,d). The actual composition of the specimen of the heat-treated alloy at 1300 °C was Cr-47.1Si-4.9Ti-2Al, i.e., it was poorer in Al and richer in Si compared with the nominal composition. Considering the XRD data (Figure 6.1) and the chemical analysis data (Table 6-2), the Ti_6Si_5, Cr_5Si_3 and $CrSi_2$ silicides were present in AN3-HT1300. However, the EDX data also confirmed the presence of CrSi. There was severe cracking of the Ti_6Si_5 silicide with the cracks being paralleled to each other see

Figure 6.2 (f). The latter figure would suggest that the $CrSi_2$ and Cr_5Si_3 were better at arresting the cracks compared with CrSi.

In the Cr_5Si_3 (HT1200) the Si+Al concentration was ~ 40.3 at.% with Al/Si≈0.04 and in the $CrSi_2$ (HT1200) the Si+Al concentration was ~ 66.5 at.% with Al/Si ≈0.25. In the Cr_5Si_3 (HT1300) the Si+Al concentration was ~ 39.7 at.% with Al/Si≈ 0.02 and in the $CrSi_2$ (HT1300) the Si+Al concentration was ~ 66.1 at.% with Al/Si ≈0.12. The reduction of the Al/Si ratios after

Table 6-2 Quantitative EDX analysis data (at. %) of the cast and heat treated AN3 alloy

Phase	Cr	Si	Ti	Al
AN3-AC[a,b]	45.7 ±0.3	44.7±0.1	6.6 ±0.4	3.1 ±0.1
	45.3-45.9	44.6-44.7	6.3-7.1	3-3.1
$(Ti,Cr)_6Si_5$	43.6 ±1.1	45.6 ±0.1	10.8 ±1.2	-
	42.5-45.0	45.5-45.7	9.3-12.0	-
$(Cr,Ti)_5(Si,Al)_3$	58.8 ±0.2	39.1 ±0.1	1.2 ±0.3	0.9 ±0.2
	58.5-59.0	39.0-39.2	0.8-1.6	0.7-1.1
$Cr(Si,Al)_2$	33.7 ±0.2	51.3 ±0.9	-	15.0±1.1
	33.4-34.0	50.1-52.6	-	13.4-16.2
AN3-HT1200[a,b]	44.5±3.1	45.4±1.7	4.9±1.2	5.2±1.8
	41.5-48.4	43.2-47.4	4.0-7.1	3.4-7.9
$(Ti,Cr)_6Si_5$	42.4±0.5	45.8±0.7	11.6±0.3	-
	42.1-42.9	45.4-46.6	11.3-11.8	-
$(Cr,Ti)_5(Si,Al)_3$	58.8±1.0	38.9±0.4	0.9±0.4	1.4±0.2
	57.4-59.6	38.6-39.5	0.6-1.4	1.2-1.6
$Cr(Si,Al)_2$	33.5±0.3	53.4±1.0	-	13.1±1.1
	33.2-33.8	52.2-54.1	-	12.3-14.3
AN3-HT1300[a,b]	46.0±0.2	47.1±0.3	4.9±0.1	2.0±0.4
	45.7-46.2	46.7-47.5	4.8-5.0	1.8-2.8
$(Ti,Cr)_6Si_5$	46.0±0.4	45.2±0.3	8.8±0.7	-
	45.4-46.5	44.7-45.7	8.0-9.9	-
$(Cr,Ti)_5(Si,Al)_3$	59.9±0.3	39.0±0.5	0.5±0.1	0.7±0.1
	59.5-60.4	38.3-40.0	0.4-0.7	0.6-0.8
$Cr(Si,Al)_2$	34.0±0.3	59.1±0.5	-	7.0±0.6
	33.5-34.3	58.6-59.7	-	6.1-7.6
Cr(Si,Al)	50.4±0.3	49.2±0.2	-	0.5±0.1
	50.0±50.8	48.8-49.4	-	0.4-0.6

[a] Large area analysis from the center of the button

[b] AC=as cast , HT1200 = heat treatment at 1200 °C/100 h, HT1300 = heat treatment at 1300 °C /100 h

the heat treatment of the alloy at 1300 ^{o}C was attributed to the formation of the CrSi phase.

6.2.1.3 As cast Cr-25Si-25Al-5Ti (alloy AN4-AC)

Data for the compositions and microstructures of the button and phases in AN4-AC is given in Table 6-3 and in Figure 6.3 and Figure 6.4 (a, b, c). The data in Table 6-3 summarizes the compositions of the phases in the bulk button. Compared with the nominal composition, the AN4-AC was richer in Al. There was also macrosegregation of Al, which was stronger compared with that in the alloy AN2-AC, see section 5.2.1.4.

According to the XRD data (Figure 6.3) and the EDX data (Table 6-3), the Ti_6Si_5, Cr_5Si_3, Cr_5Al_8 and Cr_4Al_9 phases were present in the microstructure of AN4-AC. EBSD was used to aid phase identification and confirm the crystal structures of the phases, see Figure 6.5. The MAD values were between 0.2-0.7 in the pattern matching process provided by Chanel 5 software. The Ti_6Si_5 silicides had needle-shape and often formed parallel to each other and in groups. The needles were grown perpendicular or diagonal to the Cr_5Si_3.The latter was formed adjacent to the 6-5 silicide as a round lumpy phase. The Ti_6Si_5 and Cr_5Si_3 were surrounded by the Al_8Cr_5 and Al_9Cr_4 aluminides.

In this Al rich alloy there was solubility of Al in the Ti6Si5, of about 6.8 at.%, and the maximum solubility of Ti was 14.7 at.%. In the Cr5Si3 there were Ti rich areas where the maximum Ti solubility was 6.8 at.%. The brighter and darker areas in the matrix were the Al8Cr5 and Al9Cr4 aluminides, respectively, see Figure 6.4 (c). The microstructure of AN4-AC consisted of 27.6 % Ti_6Si_5, 30 % Cr_5Si_3 and 42.4 % aluminide matrix, see Table 6-1.

6.2.1.4 Heat treated Cr-25Si-25Al-5Ti (alloy AN4-HT)

The alloy was given two different heat treatment, namely 1200 ^{o}C/100 h and 1300 ^{o}C/100 h. The actual composition of the heat-treated specimen at 1200 ^{o}C was Cr-24.9Si-25.5Al-4.6Ti, essentially the same as the nominal composition. According to the XRD (Figure 6.3) and chemical analysis data (Table 6-3), the microstructure of AN4-HT1200 consisted of the Ti_6Si_5, Cr_5Si_3, Ti_5Si_3 Cr_3Si, and Al_8Cr_5 phases. The large change in the size of Cr_5Si_3 was attributed to phase decomposition in the alloy at 1200 ^{o}C that was suggested by the DSC trace (Figure 6.6) in

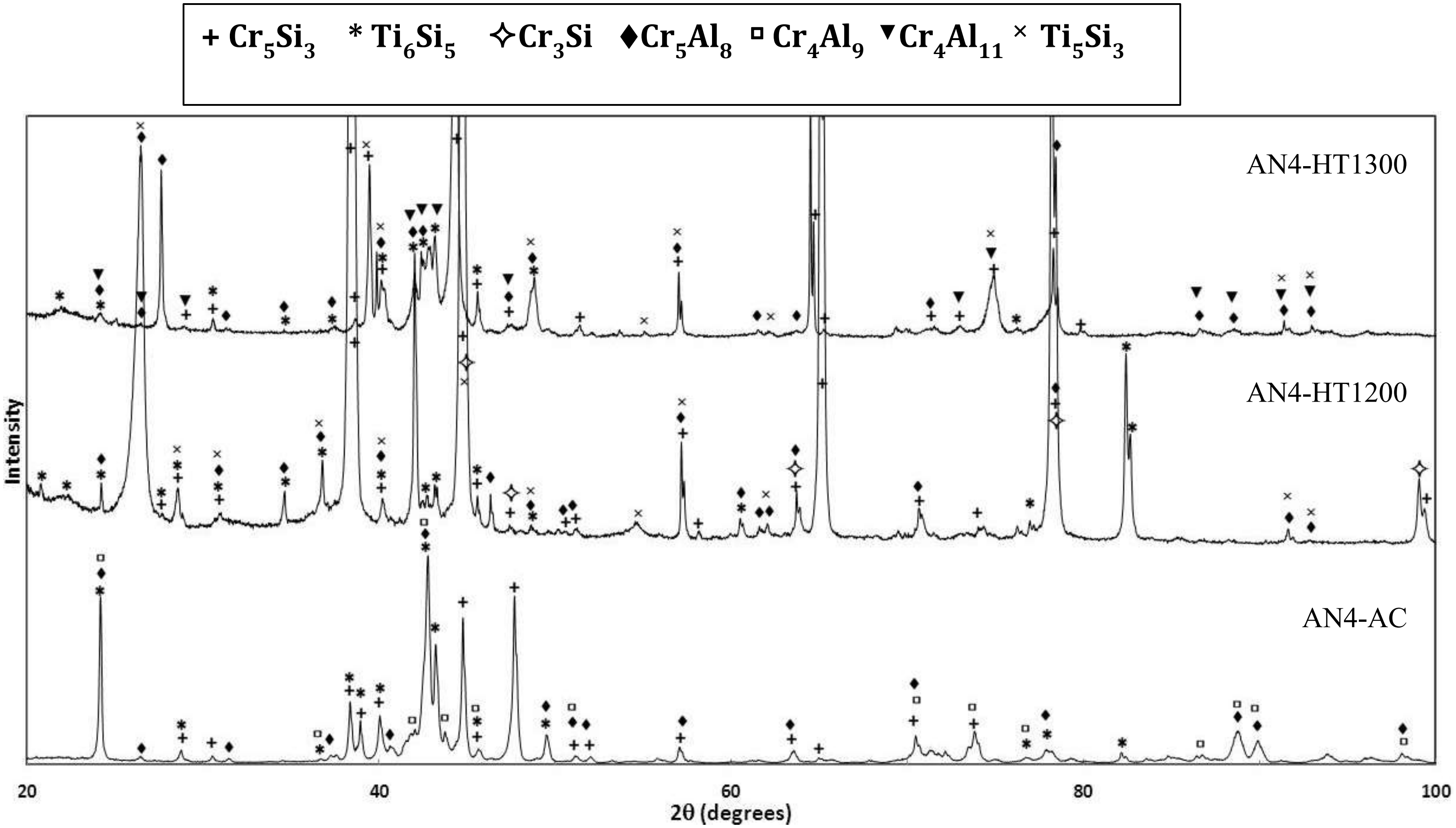

Figure 6.3 X-ray diffractograms of the as cast and heat treated alloy AN4 (card number 00-008-0041 for Ti_5Si_3, 00-050-1329 for Cr_5Si_3, 00-007-0186 for Cr_3Si 04-007-8926 for Ti_6Si_5, 00-002-1192 for Cr_5Al_8, 04-015-1130 for Cr_4Al_{11} and 00-002-1193 for Cr_4Al_9), (HT1200 = heat treatment at 1200 ^oC/100 h, HT1300 = heat treatment at 1300 ^oC /100

the temperature range 1130-1200 ^{o}C. The partitioning of Ti during the heat treatment led to the formation of Mn_5Si_3-typeTi_5Si_3 in some areas of the microstructure. There was also formation of Cr_3Si that was surrounded by a lamellar structure containing the Cr_5Si_3 intermetallic. The Ti_6Si_5 became slightly richer in Ti (Table6-3).The solubility of Al in the Cr_3Si was low and the solubility of Si in the Cr_5Al_8 was slightly reduced. Amongst the silicides formed in AN4-HT1200, the Ti_6Si_5 had the highest solubility of Al (4.6 at.%). The Cr_5Si_3 and Al_8Cr_5 were the two dominant phases in the microstructure with combined fraction 81.9 % (Table 6-1).

As the heat treatment temperature increased to 1300 ^{o}C, the fraction of Ti_6Si_5 in the microstructure was further reduced and the fraction of Ti rich Cr_5Si_3 increased to 53.7 %, see Figure 6.3 (f, g, h) and (Table 6-1). A lamellar structure containing the Cr_5Si_3 surrounded the Cr_3Si phase as was the case in AN4-HT1200. The ternary τ_3 phase of composition close to Cr_4Al_{11} was formed. There were no significant changes in the compositions of the 6-5, 5-3 and 3-1 silicides and Cr_5Al_8 aluminide compared with AN4-HT1200.

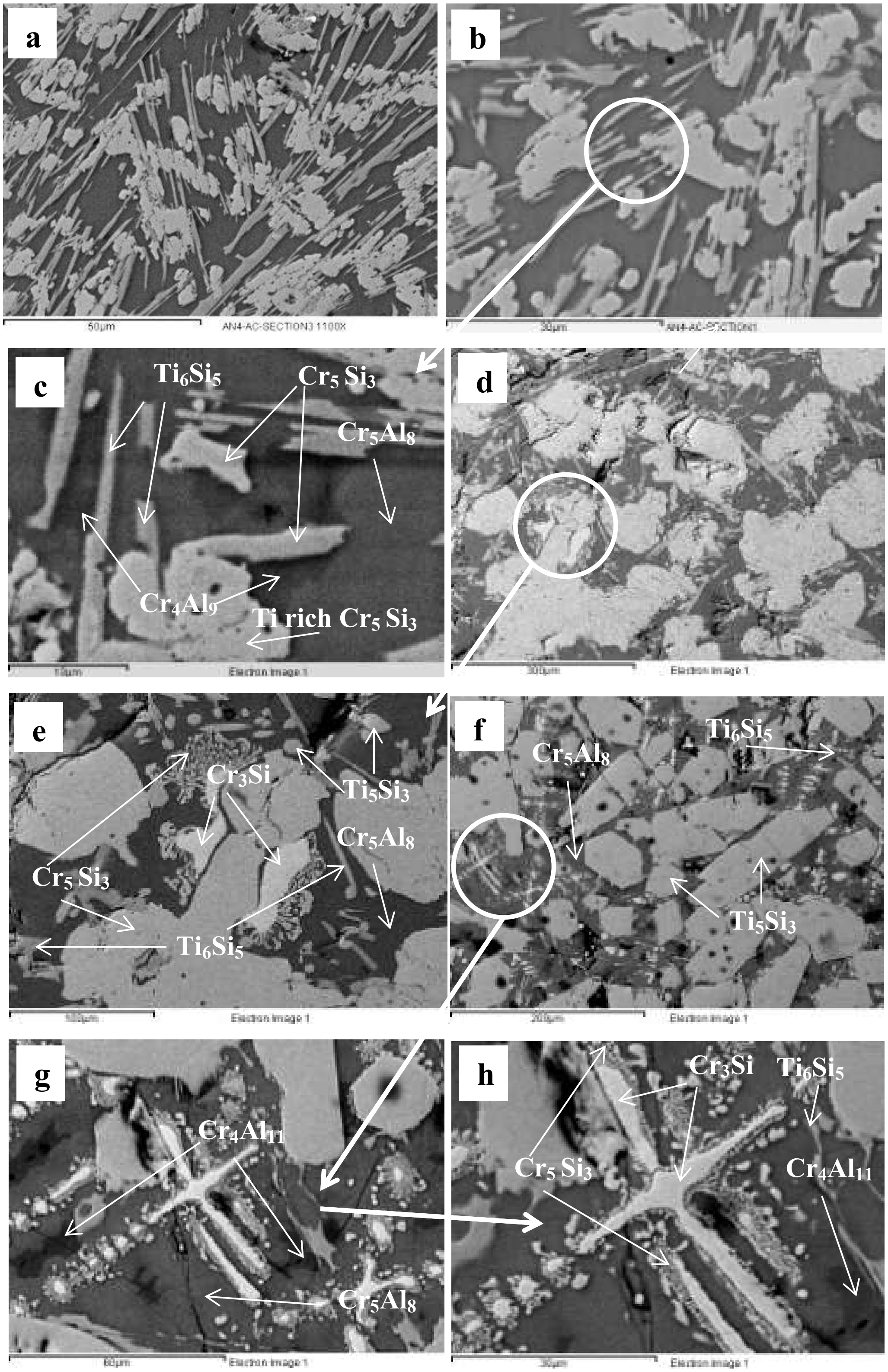

Figure 6.4 Microstructure of alloy AN4 a, b, c) as-cast d, e) heat-treated at 1200 °C for 100 h and f, g, h) heat-treated at 1300 °C for 100 h.

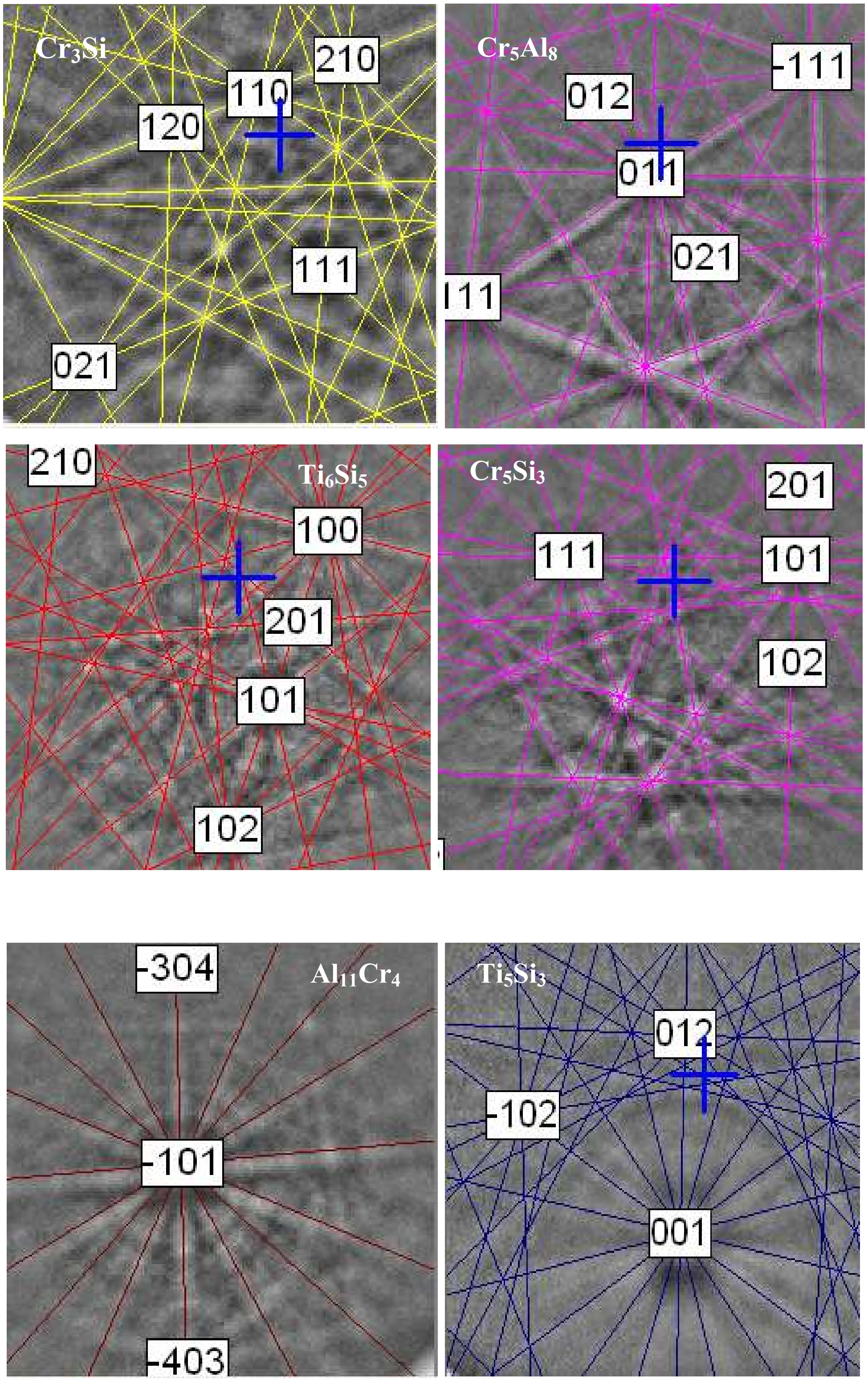

Figure 6.5 EBSD patterns of the phases in the AN4-HT1300.

Table 6-3 Quantitative EDX analysis data (at.%) of the cast and heat treated AN4 alloy

Phase	Cr	Si	Ti	Al
AN4-AC[a,b]	41.5±1.0	24.8±0.8	4.7±0.1	29.1±1.7
	40.6-43.1	24.2-26.3	4.6-4.9	25.7-30.2
$(Ti,Cr)_6(Si,Al)_5$	39.7±0.5	39.9±1.0	13.6±0.7	6.8±1.5
	38.9-40.3	37.8-40.9	12.4-14.7	5.0-9.8
(Cr,**Ti**)$_5$(Si,Al)$_3$[c]	55.3±1.0	36.1±0.5	5.8±1.0	2.9±1.0
	53.6-56.7	34.9-36.5	4.3-6.8	2.0-5.1
(**Cr**,Ti)$_5$(Si,Al)$_3$	58.6±0.9	35.6±0.8	2.4±0.8	3.1±1.3
	57.6-59.2	34.7-36.1	1.6-3.2	2.1-4.6
$Cr_5(Si,Al)_8(\gamma\text{-}_H)$	35.6±0.5	8.6±0.9	0.8±0.3	55.1±1.4
	34.5-36.3	7.2-10.4	0.5-1.5	51.9-56.6
$Cr_4(Si,Al)_9(\tau_4)$	30.7±0.6	11.6±1.3	0.6±0.3	57.3±2.6
	30.3-31.2	10.6-12.5	0.4-0.8	55.5-59.1
AN4-HT1200[a,b]	44.8±0.5	24.9±0.5	4.6±0.4	25.5±0.3
	44.5-45.1	24.5-25.3	4.3-4.8	25.3-25.8
$(Ti,Cr)_6(Si,Al)_5$	39.2±0.7	40.7±1.0	15.5±0.8	4.6±1.1
	38.2-41.0	39.1-42.6	13.8-16.9	2.8-7.9
(**Cr**,Ti)$_5$(Si,Al)$_3$	57.1±0.4	35.7±0.3	4.9±0.2	2.3±0.2
	56.4-57.7	35.0-36.2	4.6-5.3	2.0-2.8
(**Ti**,Cr)$_5$(Si,Al)$_3$[d]	44.5±0.6	35.8±0.4	17.0±0.5	2.7±0.9
	43.2-45.6	34.7-36.6	15.7-18.0	2.0-6.4
$Cr_3(Si,Al)$	74.2±0.3	24.0±0.3	0.5±0.1	1.3±0.1
	73.8-74.4	23.7-24.4	0.4-0.5	1.2-1.5
$Cr_5(Si,Al)_8(\gamma\text{-}_H)$	36.6±0.6	6.5±0.4	0.4±0.1	56.5±0.6
	35.6-37.7	5.6-7.1	0.2-0.5	55.8-58.0
AN4-HT1300[a,b]	41.5±1.0	24.8±0.8	4.7±0.1	29.1±1.7
	40.6-43.1	24.2-26.3	4.6-4.9	25.7-30.2
$(Ti,Cr)_6(Si,Al)_5$	40.7±0.3	40.5±0.1	13.7±0.6	5.1±0.5
	40.4-41.0	40.3-40.6	12.8-14.2	4.7-5.9
(**Cr**,Ti)$_5$(Si,Al)$_3$	54.3±1.4	34.3±1.1	4.9±0.1	6.5±2.5
	53.3-55.3	33.5-35.1	4.9-5.0	4.8-8.3
(**Ti**,Cr)$_5$(Si,Al)$_3$[d]	45.7±0.7	36.3±0.4	15.8±0.6	2.1±0.2
	44.5-46.9	35.7-37.3	15.0-17.1	1.7-2.3
$Cr_3(Si,Al)$	73.1±0.6	24.0±0.8	0.6±0.1	2.3±1.0
	72.2-73.9	22.3-25.0	0.5-0.8	1.5-4.8
$Cr_4(Si,Al)_{11}(\tau_3)$	26.9±0.7	6.3±0.4	0.6±0.1	66.2±0.8
	25.7-27.4	5.8-6.7	0.5-0.8	65.4-67.3
$Cr_5(Si,Al)_8(\gamma\text{-}_H)$	36.0±0.9	7.1±0.4	0.9±0.1	56.1±1.3
	34.9-36.9	6.6-7.6	0.8-1.0	54.6-57.8

[a] Large area analysis from the centre of the button

[b] AC=as cast , HT1200 =heat treatment at 1200 °C/100 h, HT1300 =heat treatment at 1300 °C /100 h.

[c] Ti rich Cr_5Si_3 phase

[d] Mn_5Si_3 type $(Ti,Cr)_5Si_3$ (based on the XRD and EBSD data, this silicide is considered to be of the Mn_5Si_3 type)

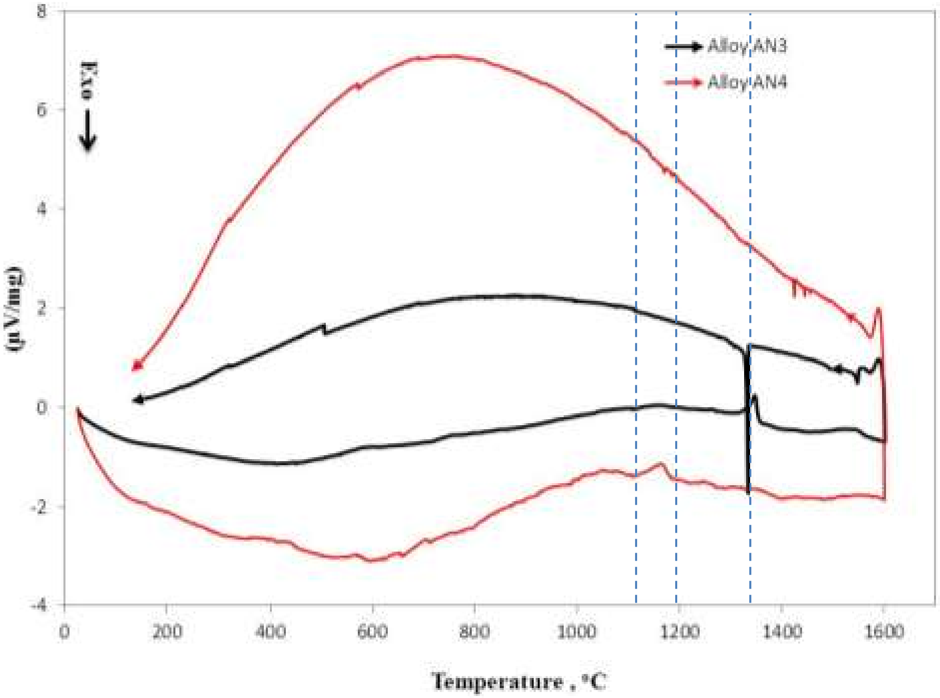

Figure 6.6 DSC trace of the alloys AN3 and AN4 obtained at 20 $Kmin^{-1}$ heating rate in flowing Argon

6.2.2 Isothermal oxidation of the as cast alloys AN3 and AN4

Oxidation experiments were performed at 800, 1000 and 1200 °C under constant air flow of 20 ml/min. Oxidation kinetics and the morphology of the oxides are presented in the following sections. The supplementary information about the measurement of oxidation kinetics is given in the Appendix A.

6.2.2.1 Oxidation kinetics of the cast alloy AN3 and AN4

Figure 6.7 and Figure 6.8 respectively show the mass change versus time at 800 °C, 1000 °C and 1200 °C and the oxidation kinetics data of the alloys, respectively. The mass change increased with temperature. The data showed that parabolic (n=0.5) and near parabolic (0.45 < n <0.55) oxidation, paralinear (two stage oxidation consisting of parabolic and linear behaviour; n=0.5, n=1) was obeyed. The weight change data was analysed using the equations 6.1 and 6.2 :

$(\Delta m/A)= K t^n$ Equation 6.1

$\ln(\Delta m/A) = \ln K + n \ln t$ Equation 6.2

where $\Delta m/A$ is the weight change per unit area, t is the reaction time and K and n are constants. The oxidation reaction kinetics was then characterized as parabolic etc. depending on the value of the exponent n. The n value for the alloy AN3 and AN4 was taken from the equations $y1=0.014t^{0.48}$, $y2=0.039t^{0.45}$, $y3=0.092t^{0.47}$ (see Figure 6.8 a) and $y1=0.005t^{0.51}$, $y2=0.019t^{0.47}$, $y3=0.078t^{0.46}$ (see Figure 6.8 b)respectively for 800, 1000 and 1200 °C. The calculated parabolic rate constants kp, see Figure 6.8 b, are given in Table 6-4. The results show that the rate constants increased with increasing oxidation temperature.

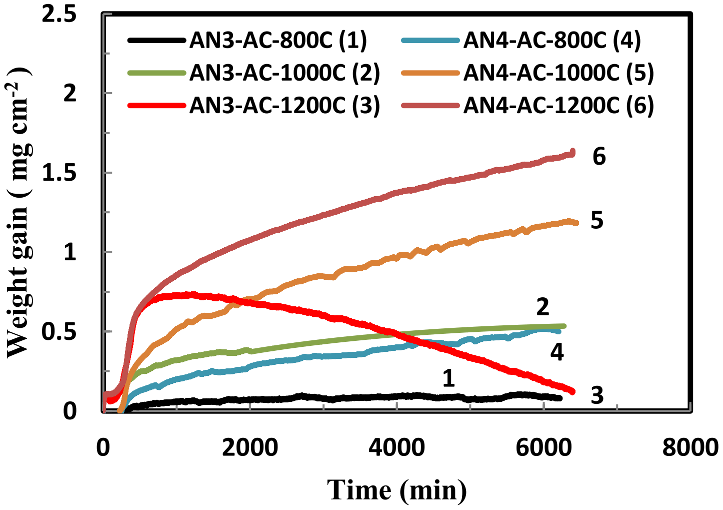

Figure 6.7 Weight change of the alloys AN3 and AN4 after isothermal oxidation in air at 800, 1000 and 1200 °C.

Considering the n values of the alloys AN3 and AN4, it is concluded that both alloys followed parabolic oxidation kinetics at 800 °C, 1000 °C and 1200 °C with the exception of the alloy AN3 at 1200 °C which obeyed paralinear oxidation kinetics at longer exposure times (t>16 h), The overall oxidation kinetics in this particular case could be obtained using Equation 6.3 [136]:

$(\Delta m/A)= k_p t^{0.5} - k_l t$ Equation 6.3

where the k_p and k_l are the parabolic and linear oxidation rate constants. In equation 6.3, the first component is responsible for parabolic weight gain and the second component is responsible for simultaneous weight loss of the alloy.

In this study, for comparison purposes, only the parabolic sections of curves were chosen .As shown in Table 6-4, the n values were in the range $0.45<n<0.52$ for AN3 and AN4 at 800, 1000 and 1200 °C. An interesting observation that can be made from the plots in Figure 6-8 is that the alloys AN3 and AN4 showed near-parabolic oxidation kinetics ($0.48<n<0.52$) for considerably longer time at 800 °C and 1000 °C. However, the alloy AN3 followed parabolic oxidation

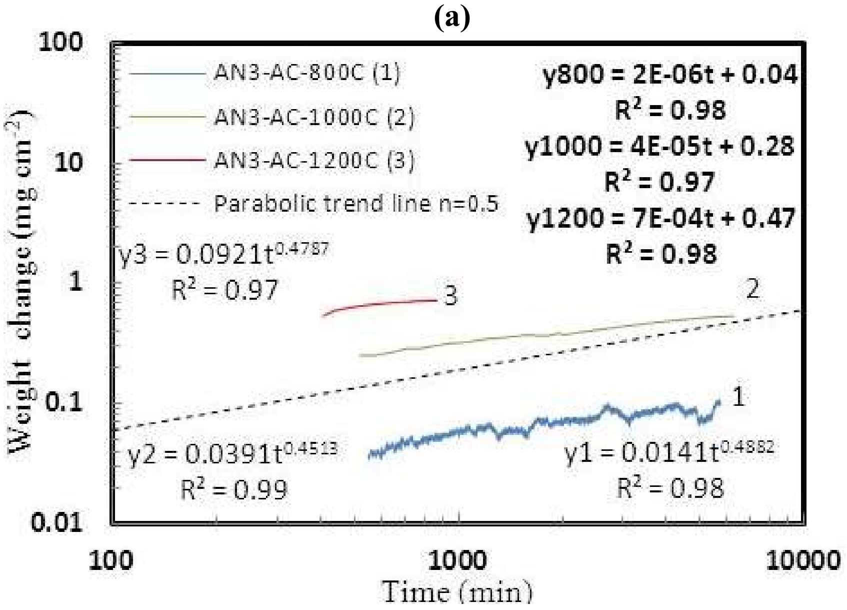

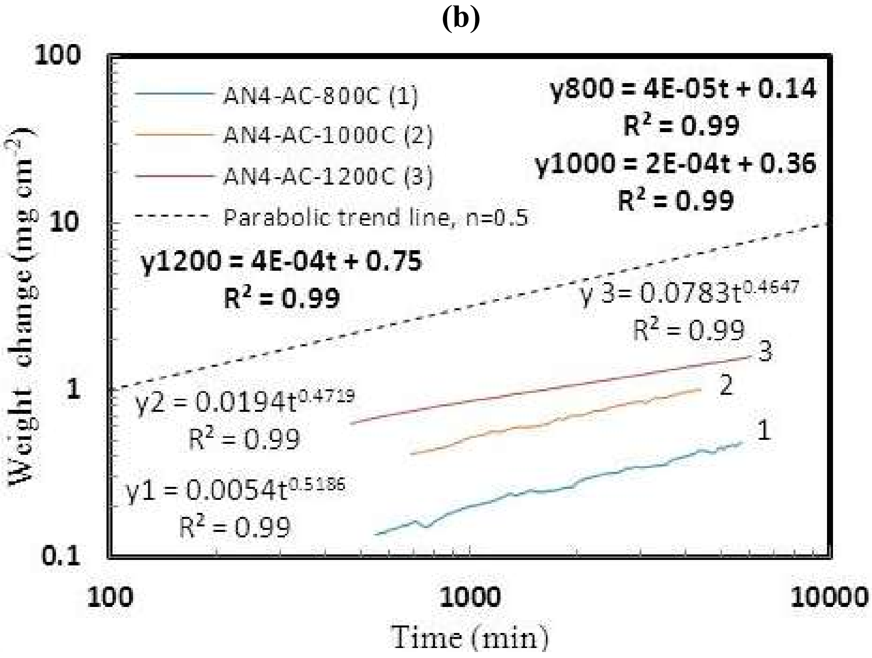

Figure 6.8 Log –log plots of weight change versus exposure time for the a) AN3 and b) AN4 alloy at 800, 1000 and 1200 °C. The value of the exponent n in equation 6.1 was obtained from these plots. Dotted lines show n=0.5 (parabolic kinetics).

kinetics at 1000 °C in the early stages of exposure (change of slop of the plot (2) in Figure 6-8 a). At 1200 °C both alloys showed parabolic oxidation kinetics up to about 17 hours followed by linear weight loss in the curve of alloy AN3 and near-parabolic weight gain in alloy AN4.

The activation energies for oxidation were obtained from the Arrhenius equation 6.4 [112]:

$$k_p = k_0 . \exp(-Q_A/RT) \qquad \text{Equation 6.4}$$

where k_p is the parabolic rate constant ($g^2cm^{-4}s^{-1}$), k_0 is the pre-exponential factor, R is the gas constant (8.3144 J/Kmol), T is the absolute temperature (Kelvin) and Q_A is the activation energy of overall reaction (kJ/mol). The parabolic oxidation rate constants, k_p, for the alloy AN3 and AN4 alloy for the three temperatures are plotted in the Arrhenius plot in Figure 6.9.

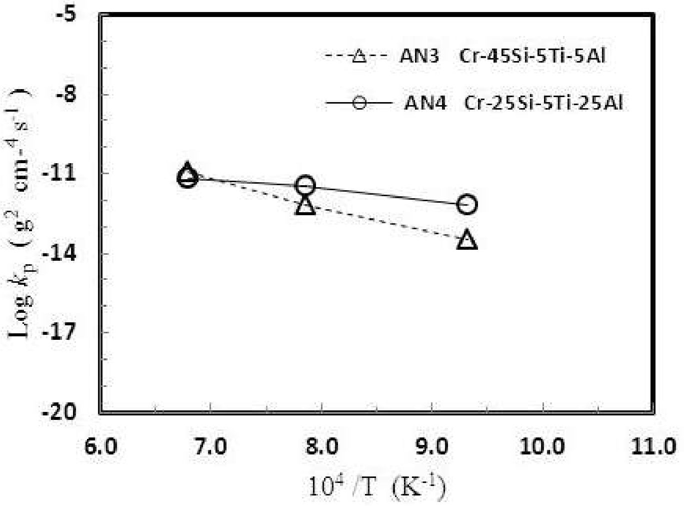

Figure 6.9 Arrhenius plots showing the variation of parabolic rate constants versus temperature, T (K) for the cast alloys AN3 and AN4.

Table 6-4 Total weight gains, oxidation rate constants and n values of the alloys AN3 and AN4 at 800, 1000 and 1200 °C

Alloy	Weight gain (mg/cm^2)	k_p ($g^2.cm^{-4}.s^{-1}$)	n
AN3-800 °C	0.11	3.3 x10^{-14} (t = 100 h)	0.4882
AN3-1000 °C	0.39	6.7x10^{-13} (t = 100 h)	0.4513
AN3-1200 °C	0.74	1.2x10^{-11} (t < 16 h)	0.4787
AN4-800 °C	0.52	6.7 x10^{-13} (t =100 h)	0.5186
AN4-1000 °C	1.43	3.3 x10^{-12}(t =100 h)	0.4719
AN4-1200 °C	1.86	6.7 x10^{-12} (t =100 h)	0.4647

Figure 6.9 shows that in each alloy a single mechanism was operative in the entire temperature range of oxidation. The activation energies of oxidation of AN3 and AN4 alloy were 90.3 and 32.4 kJ/mol, respectively (Table 6-5). The activation energy for the alloy AN3 is approximately 3 times that of AN4. This indicated that the alloy AN4 possessed better oxidation than the alloy AN3.

Table 6-5 Activation energies for the oxidation of the alloys AN3 and AN4.

Alloy	**(Temperature range** °C)	**Activation energy (kJmol** $^{-1}$)
AN3-AC	800-1200	90.3±4.4
AN4-AC	800-1200	32.4± 3.3

6.2.2.2 Oxide scale characterization

Secondary electron (SE) micrographs of the surfaces of oxidized specimens of the alloys AN3 and AN4 at 800, 1000 and 1200 ^{o}C are shown in Figures 6.10 and 6.11. The GAXRD data for the alloy AN3 and AN4 is shown in the figures 6.12 and 6.13 respectively. At 800 ^{o}C the alloy AN3 formed a non-uniform alumina oxide scale along the patches of silica scale, where facetted silicide was observed. According to the GAXRD data in Figure 6.12 (a), there was also chromia in the scale. Therefore, at 800 ^{o}C the scale formed on AN3 consisted of a mixture of oxides. Figure 6.10 a2 shows alumina flakes in the scale and Figure 6.10 a3 shows a patch of cellular silica and chromia respectively.

At 1000 ^{o}C, a rough scale resulted from the different growth rates of oxides, as shown in Figure 6.10 b2 and b3. In some areas, spallation of scales occurred and voids were seen. According to the GAXRD data (Figure 6.12 b), the most dominant oxide was alumina and there were patches of chromia and silica oxides in the outer surface of the scale.

At 1200 ^{o}C there was uniform formation of thin alumina scale (Figure 6.12 c) with weak adherence to the substrate (Figure 6.10 c).This may be result of the residual stress produced in the scale/substrate interface due to the thermal expansion miss-match of scale and substrate caused spallation. In some areas, the scale had spalled entirely (Figure 6.10 c1, c2, c4) and in the other regions a macro-crack was formed (Figure 6.10 c2) probably during the cooling of the specimen to ambient temperature. Voids beneath the alumina scale were observed. The distribution and morphology of voids were different compared with those formed at 1000 ^{o}C.

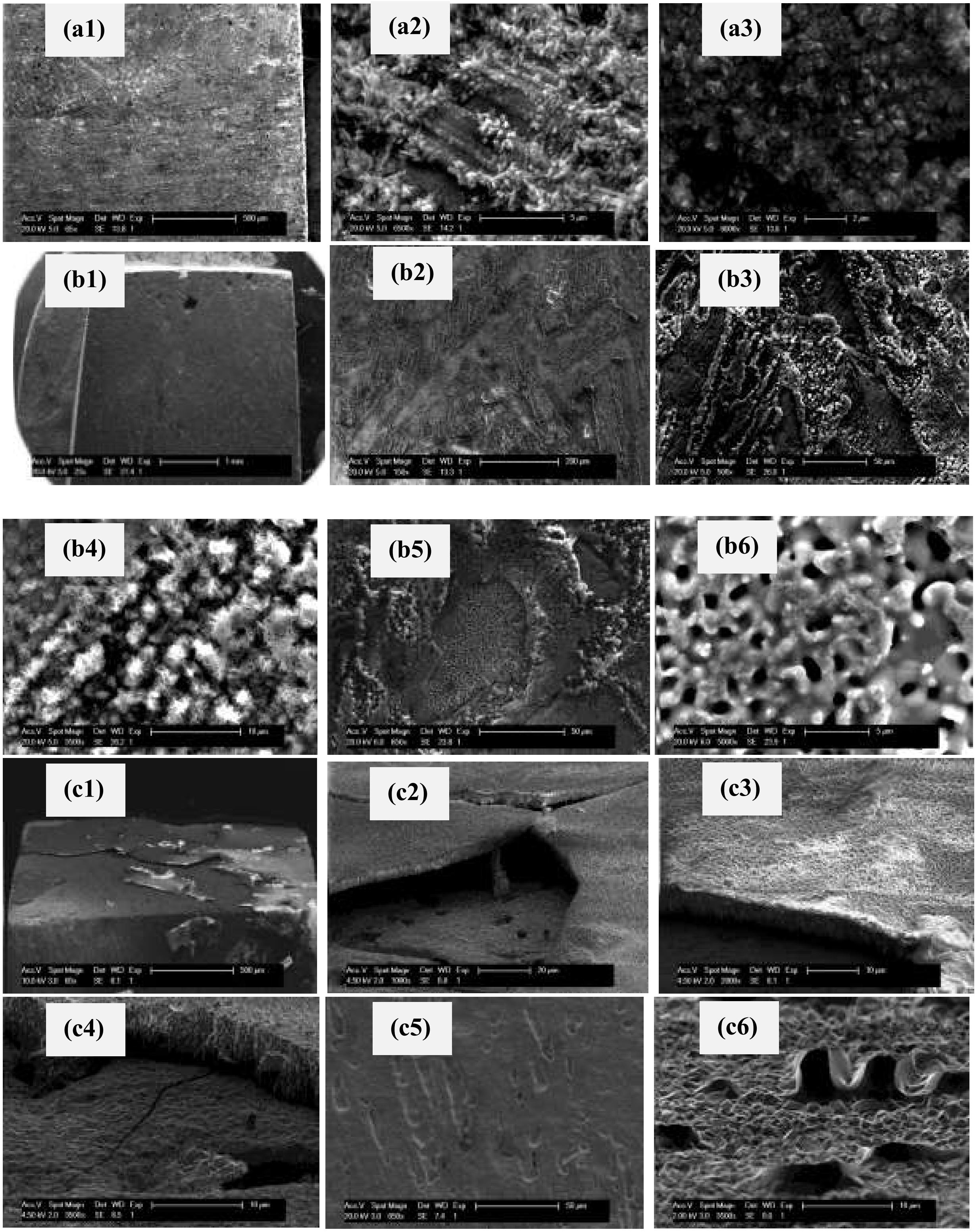

Figure 6.10 SEM-SE images of oxide scales formed on the AN3 alloy after 100 h oxidation in air at a) 800 °C, b) 1000 °C and c) 1200 °C .

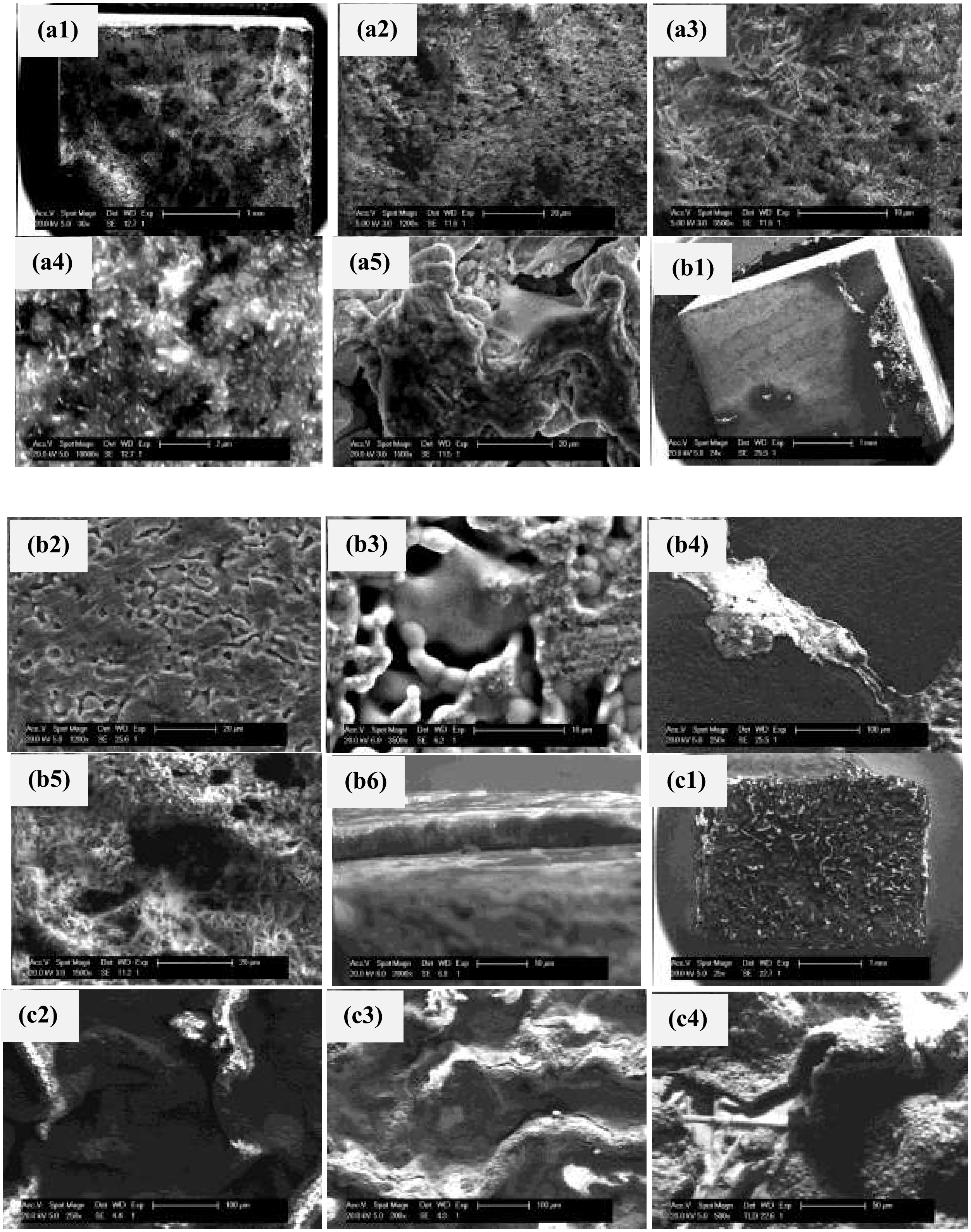

Figure 6.11 SEM-SE image of oxide scale formed on the AN4 alloy after 100 h oxidation in air at a) 800 °C, b) 1000 °C and c) 1200 °C.

Figure 6.11 shows the scale formed on the oxidized samples of AN4. At 800 ^{o}C, an almost uniform alumina oxide scale formed on the surface with patches of silica (Figure 6.13 a). In Figure 6.11 a1 and a2 the dark areas correspond to chromia and silica oxides. Alumina flakes are shown in Figure 6.11 a3 that were formed adjacent to the silica and chromia patches. The phase exhibiting bright contrast in Figure 6.11 a4 was chromia surrounded by silica. According to the cross section studies, there was no evidence of sub scale formation at 800 ^{o}C, see Figure 6.14. The formation of alumina and silica was confirmed using GAXRD, see Figure 6.13 a.

By increasing the exposure temperature to 1000 ^{o}C, the scale consisted of uniform alumina oxide (Figure 6.13 b) and was partially left on the surface of the specimen (Figure 6.11 b6). The kp value of oxidation can also confirm the protective nature of the scale during isothermal oxidation at 1000 ^{o}C. The scale was quite smooth and there was no convolution on the outer surface. The

(a)

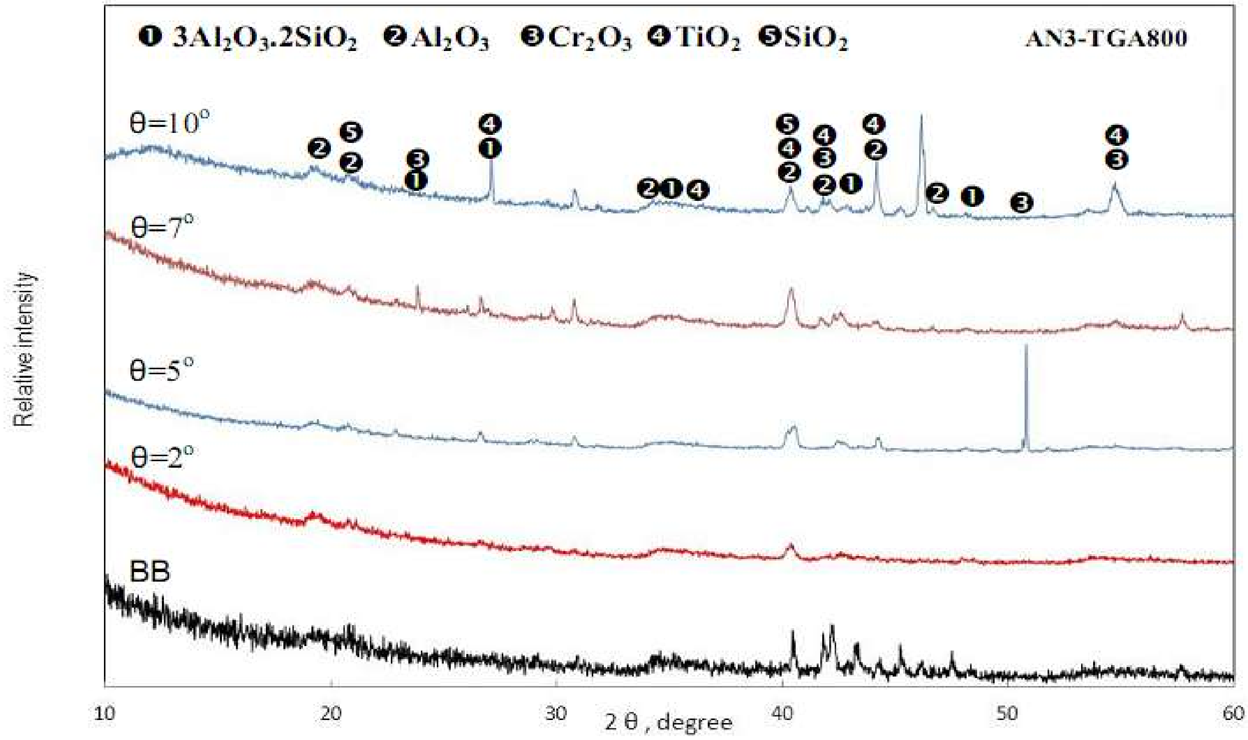

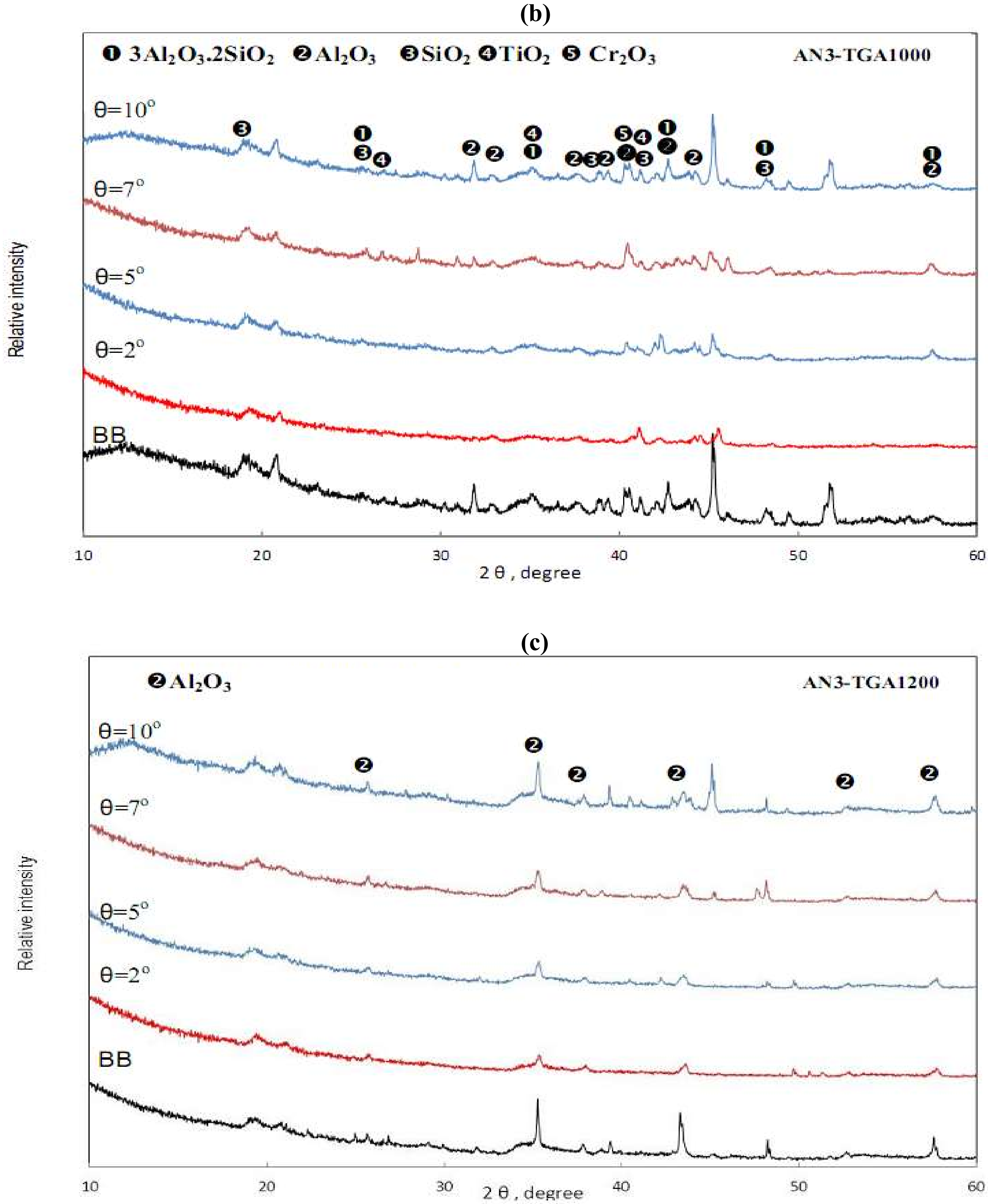

Figure 6.12 Glancing angle XRD data at different incident beam angles (θ) of the scale formed on the oxidized AN3 specimen at (a) 800 °C, (b) 1000 °C and (c) 1200 °C (BB refer to Bragg Brentano geometry diffraction pattern taken from TGA cube sample before isothermal oxidation experiment)

(a)

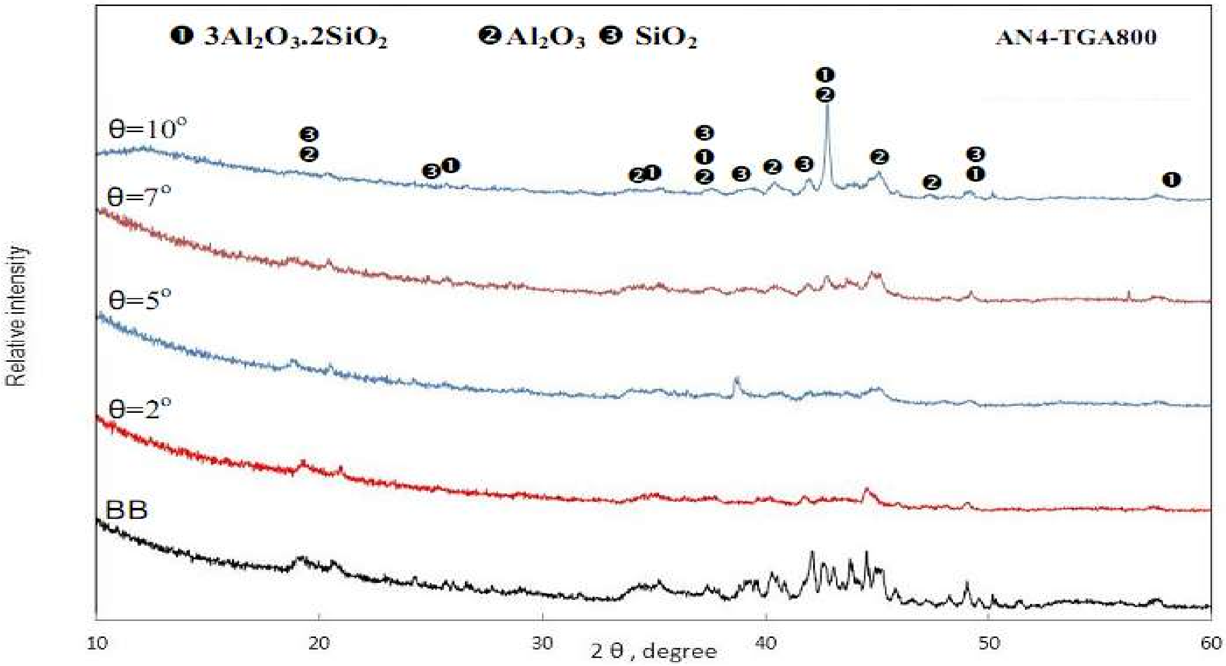
❶ $3Al_2O_3.2SiO_2$
❷ Al_2O_3 ❸ SiO_2
AN4-TGA800
θ=10°
θ=7°
θ=5°
θ=2°
BB
Relative intensity
2 θ , degree
10
20
30
40
50
60

(b)

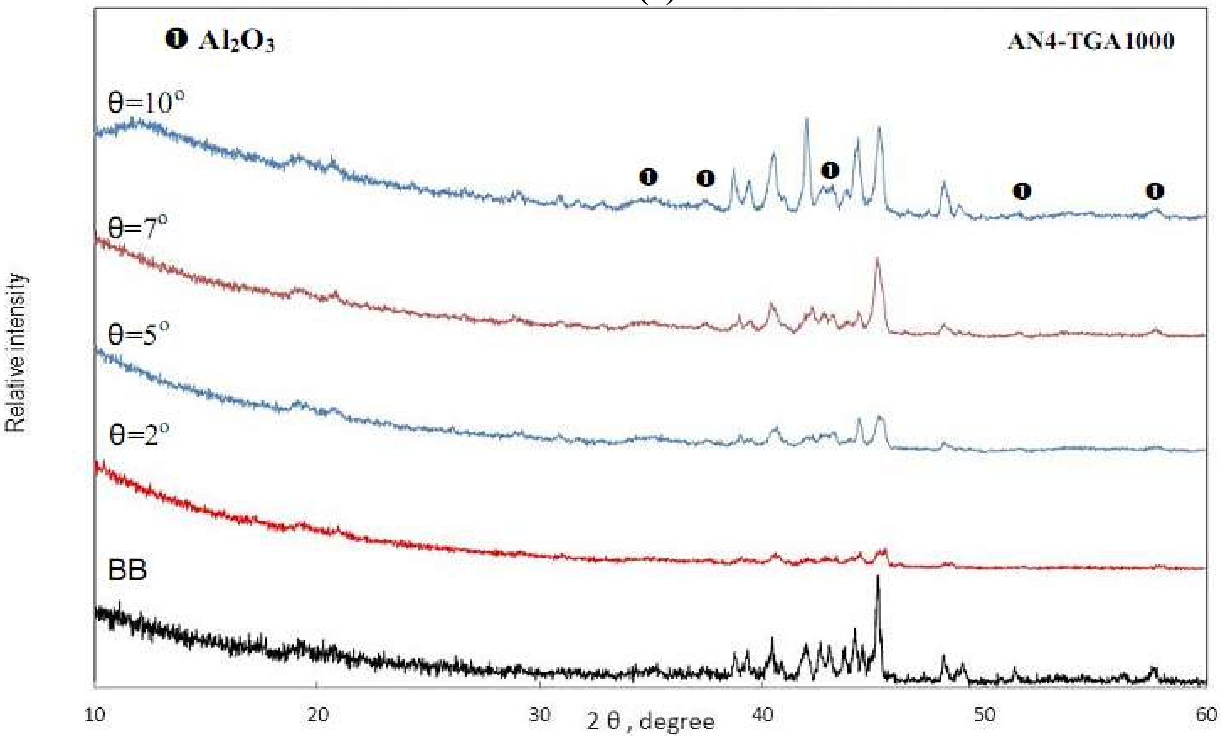
❶ Al_2O_3
AN4-TGA1000
θ=10°
θ=7°
θ=5°
θ=2°
BB
Relative intensity
2 θ , degree
10
20
30
40
50
60

(c)

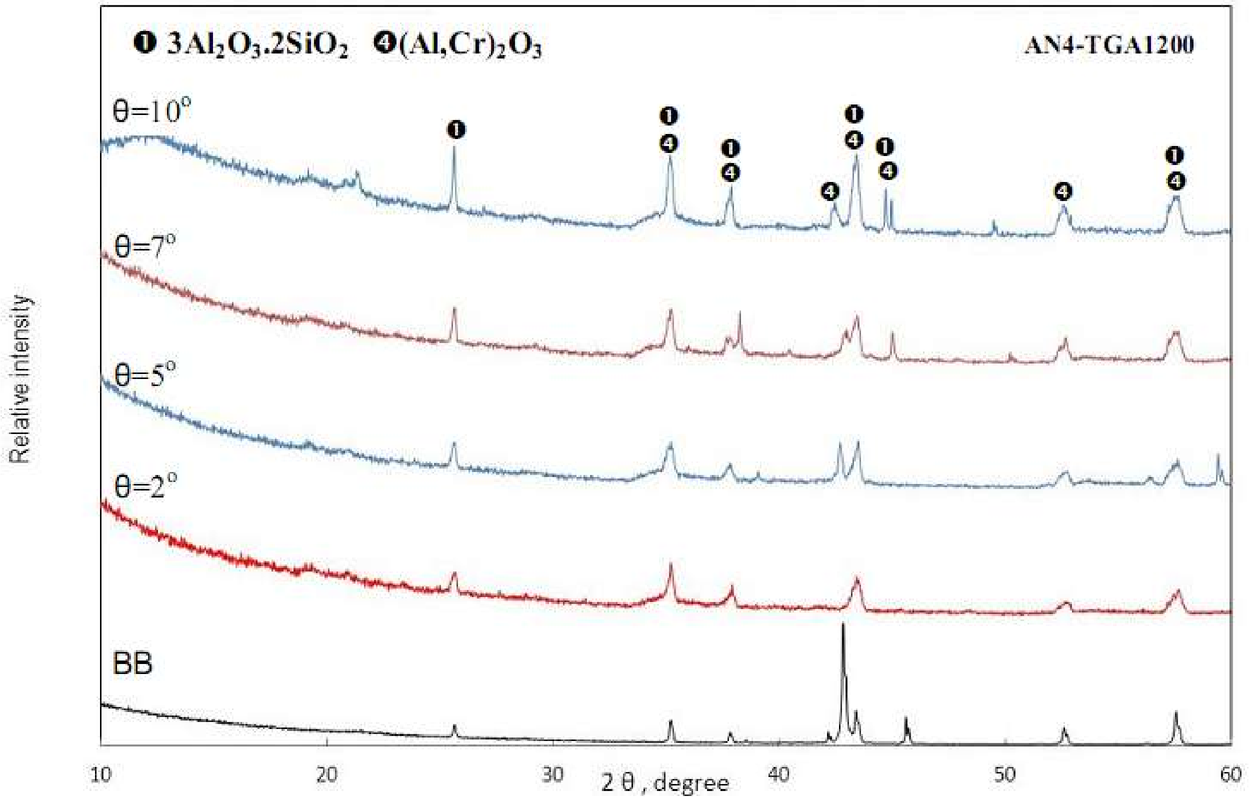

Figure 6.13 Glancing angle XRD data at different incident beam angles (θ) of the scale formed on the oxidized AN4 specimen at (a) 800 ^{o}C, (b) 1000 ^{o}C and (c) 1200 ^{o}C (BB refer to Bragg Brentano geometry diffraction pattern taken from TGA cube sample before isothermal oxidation experiment)

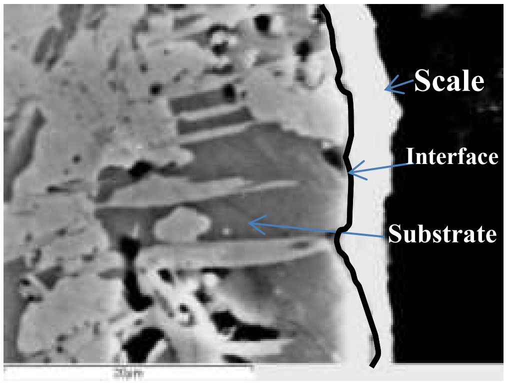

Figure 6.14 cross section of the oxidized alloy AN4 at 800 ^{o}C (solid line represents the interface between scale and substrate)

thickness of the uniform scale was about 5µm. Geometrical voids were formed all over the specimen at the substrate/oxide interface, see Figure 6.11 b2 and b3. The density of voids was higher in some areas. Figure 6.11 (b6) shows the continuous alumina scale being very adherent to the substrate.

At 1200 ^{o} C, the scale surface was highly corrugated as shown in Figure 6.11 (c1-c4),. The outer scale was alumina (Figure 6.13 c) and was continuous on the surface of the specimen. The scale had spalled and broken on the ridge. The cracks on the scale could be attributed to the formation of wrinkles on the scale that caused residual stresses in the scale that led to rupture. This suggests that due to the strong adherence of the scale to the substrate, the growth and thermal stresses were relieved by substrate deformation. The second important conclusion is that in later stages of the reaction, voids and subsequently cracks began to form in the scale. Oxygen penetrated into the scale through these physical defects contributing to the overall growth of the scale.

6.3. Discussion

6.3.1 Microstructures of Cr-45Si-5Al-5Ti (alloy AN3)

The microstructure of AN3-AC consisted of the T ($(Ti,Cr)_6Si_5$), T1 ($(Cr,Ti)_5(Si,Al)_3$) and $Cr(Si,Al)_2$ silicides (Table 6-2) with the fraction of T being the highest and that of T1 the lowest (Table 6-1). The melting temperatures of unalloyed Cr_5Si_3 and $CrSi_2$ are respectively 1666 ^oC and 1439^oC, see section 2.2. There is no data regarding the melting temperature of the T ($(Ti,Cr)_6Si_5$) phase. According to Du and Schuster [21] (i) their proposed isothermal sections for the Cr-Si-Ti system at 800, 1000 and 1600 ^oC show that the T phase ($(Ti,Cr)_6Si_5$) is not stable at 1600 ^oC at which temperature the T1 ($(Cr,Ti)_5Si_3$) can be in equilibrium with the melt, (ii) their reaction scheme for the Cr-Si-Ti system shows that the T1 forms before the T phase, and (iii) their calculated isopleth at 5 at. % Ti from 40 to 90 at.% Si shows (a) that above ~ 52 at% Si the T is the primary phase and the T1 phase cannot form, (b) that the CrSi2 can form with T and T1 below ~ 48 at% Si and (c) that between 48 and 52 at% Si the $CrSi_2$ and CrSi can exist with the T phase but not the T1 which is stable above 1400 ^oC.

If we were to consider Al together with Si in the alloy AN3, in other words consider this alloy AN3 as Cr-50Si-5Ti then the above data would suggest that the solidification path in AN3-AC of the nominal composition would be L → L + T1 → L + T1 + T → L + T + CrSi → CrSi + T + $CrSi_2$. If were to use the actual Si+Al content of the AN3-AC given in Table 6-2, which is 47.8 at% Si, then the above data would suggest that the solidification path in AN3-AC would be L → L + T1 → L + T1 + T → T + CrSi + T1. Both paths (1) give the T1 as the primary phase, (2) give the CrSi in the final microstructure (the CrSi was not observed in AN3-AC) and (3) depending on Si content the T1 or $CrSi_2$ are predicted to be present in the final microstructure.

The above solidification path for AN3-AC can be compared with the calculated paths using the Pandat and ThermoCalc SSOL4 databases. The former database gives (with comments by the author in parenthesis) the solidification path shown in Figure 6.15.

1947 K LIQUID -→ Ti_5Si_3 (meaning hexagonal 5-3 silicide with prototype Mn_5Si_3)

1702 K LIQUID + $Ti_5Si_3 \rightarrow Mo_5Si_3$ (meaning tetragonal 5-3 silicide with prototype W_5Si_3, i.e., isomorphous with Cr_5Si_3, or T1, see above and section 2.2)

1656 K LIQUID $\rightarrow Mo_5Si_3$ + T

1623 K LIQUID + $Mo_5Si_3 \rightarrow$ T + CrSi

1618 K LIQUID $\rightarrow$ T + CrSi + $CrSi_2$

1505 K LIQUID $\rightarrow$ CrSi + $CrSi_2$

1175 K CrSi + $CrSi_2$

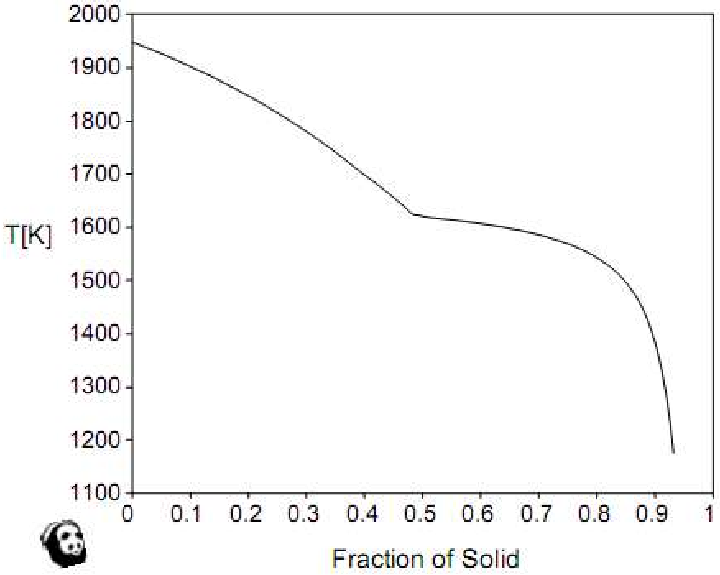

Figure 6.15 Solidification path for the alloy AN3-AC using Pandat database.

and the latter gives the solidification path for the alloy shown in Figure 6.16 (the $TiSi_2$ is not isomorphous with the $CrSi_2$ (C40 structure)).

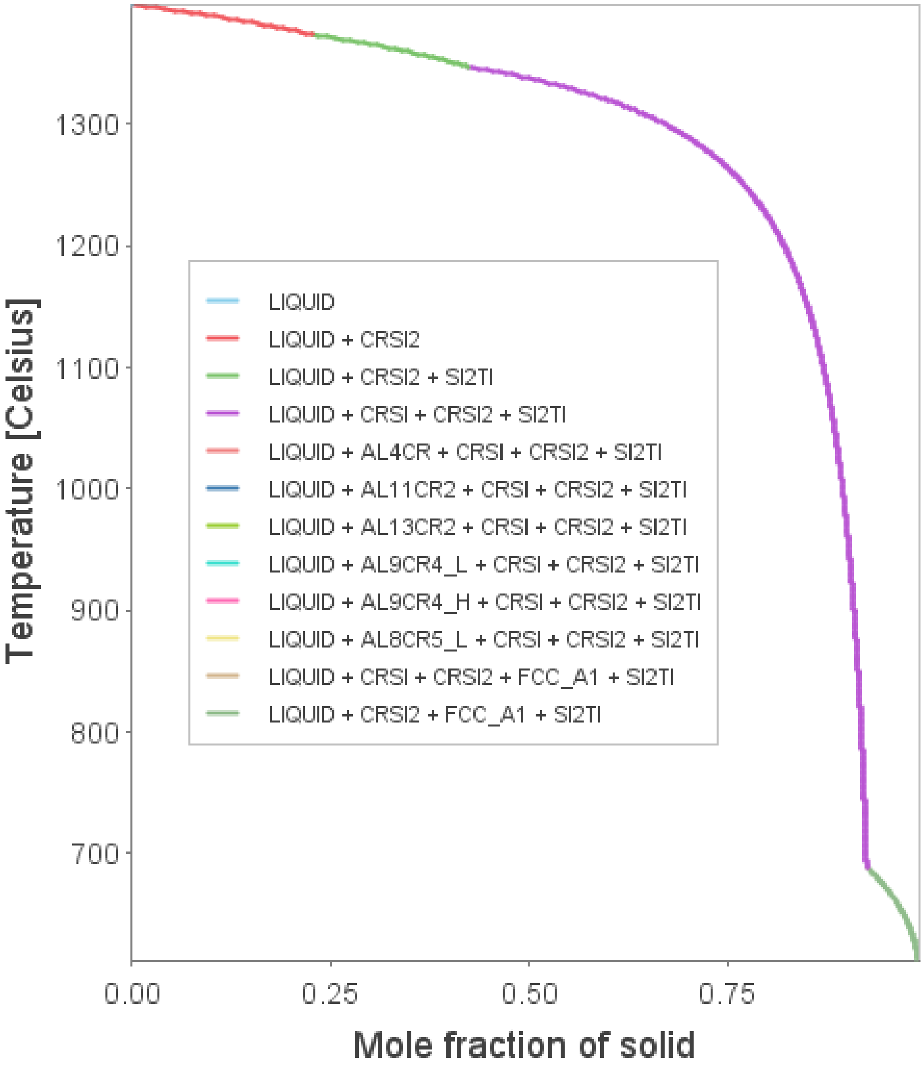

Figure 6.16 Solidification path for the alloy AN3-AC using ThermoCalc SSOL4 database

The Pandat database gives a 5-3 silicide as the primary phase followed with the formation of the T phase but predicts that the T1 and T are not stable in the final microstructure that is predicted to consist of the CrSi and $CrSi_2$ silicides. The ThermoCalc SSOL4 database cannot account for the formation of the T1 and T silicides, predicts the formation of Cr aluminides, $TiSi_2$ and Al and the CrSi and $CrSi_2$ silicides, of which the latter is predicted to exist in the final microstructure together with Al and $TiSi_2$.

The actual microstructure of AN3-AC would thus suggest that the synergy of Ti with Al, Cr and Si suppressed the formation of CrSi during solidification. However, as we shall discuss below this silicide is stable in AN3 at 1300 ^{o}C.

The above discussion would point to T1 being the primary phase in AN3-AC rather that the T. If we were to accept this, then the EDX data for the phases in AN3-AC given in Table 6-2 shows that as the T1 formed first the surrounding melt became lean in Cr and rich in Al, Si and Ti, then the T phase was formed that consumed all the Ti and made the remaining melt rich in Al and in this melt the $Cr(Si,Al)_2$ was finally formed. If we were to consider the compositions of phases to account for a sequence of phase formation where the T was the primary phase, in this case as the T phase formed the surrounding melt became lean in Ti and rich in Al, in this melt the T1 was formed consuming all the Ti and making the surrounding melt lean in Cr and rich in Al and Si and in this melt the $Cr(Si,Al)_2$ was formed.

The microstructure of AN3-HT1200 consisted of the T ($(Ti,Cr)_6Si_5$), T1 ($(Cr,Ti)_5(Si,Al)_3$) and $Cr(Si,Al)_2$ silicides (Table 6-2) with changes in the fractions of all three phases compared with the cast alloy (Table 6.1) with no evidence of the Cr(Si,Al). In the 1000 ^{o}C isothermal section of the Cr-Si-Ti system (the closest isothermal section to 1200 ^{o}C that is available in the literature, see Figure 2.16 (b) [21]) an alloy of composition Cr-50.6Si-5Ti (the actual composition of AN3-HT1200, see Table 6-2) falls in the $CrSi_2$-CrSi-T1 three phase field.

The microstructure of AN3-HT1300 consisted of the T ($(Ti,Cr)_6Si_5$), T1 ($(Cr,Ti)_5(Si,Al)_3$), $Cr(Si,Al)_2$ and Cr(Si,Al) silicides (Table 6-2) with small changes in the fractions of the T and T1 phases (compared with AN3-HT1200) and decrease in the fraction of $Cr(Si,Al)_2$ to account for the formation of the Cr(Si,Al) (Table 6-1). In the 1000 ^{o}C isothermal section of the Cr-Si-Ti system (the closest isothermal section to 1300 ^{o}C that is available in the literature, see Figure 2.16 (b) [21]) an alloy of composition Cr-49.1Si-5Ti (the actual composition of AN3-HT1300, see Table 6-2) falls in the $CrSi_2$-CrSi-T1 three phase field or the CrSi-T1 two phase field. Longer heat treatment times at 1300 ^{o}C are required to confirm the equilibrium microstructures at 1200 and 1300 ^{o}C.

6.3.2 Microstructures of Cr-25Si-25Al-5Ti (alloy AN4)

The microstructure of AN4-AC consisted of the T ($(Ti,Cr)_6Si_5$), T1 ($(Cr,Ti)_5(Si,Al)_3$) silicides and the $Cr_5(Si,Al)_8$ and $Cr_4(Si,Al)_9$ aluminides (Figure 6.4 and see composition of constituents in Table 6-3) with the fraction of $Cr_5(Si,Al)_8$ being the highest and very similar fractions of the T1 and $Cr_4(Si,Al)_9$ (Table 6-1). The melting temperatures of unalloyed Cr_5Si_3, Cr_5Al_8 and Cr_4Al_9 are respectively about 1666 ^oC, 1350 ^oC and 1170 ^oC, see sections 2.2 and 2.3. There is no data regarding the melting temperature of the T ($(Ti,Cr)_6Si_5$) phase (see above, section 6.3.1). According to Liang et al. [16,40] in Cr-Al-Si alloys the Cr_5Al_8 is formed form liquid and Cr_3Si at 1194 ^oC where it is at equilibrium with Cr_5Si_3.

The solidification path for AN4-AC can be compared with the calculated paths using the Pandat and ThermoCalc SSOL4 databases. The former database gives the solidification path shown in Figure 6.17 (with comments by the author in parenthesis).

2031 K LIQUID → Ti_5Si_3 (meaning hexagonal 5-3 silicide with prototype Mn_5Si_3)

1698 K LIQUID + Ti_5Si_3 → Mo_5Si_3 (meaning tetragonal 5-3 silicide with prototype W_5Si_3, i.e., isomorphous with Cr_5Si_3, or T1, see above and section 2.2)

1645 K LIQUID → Mo_5Si_3 + A15_Nb_3Al (meaning Cr_3Si as this is also an A15 phase)

1420 K LIQUID + Mo_5Si_3 + A15_Nb_3Al

final microstructure consisting of Mo_5Si_3 + A15_Nb_3Al

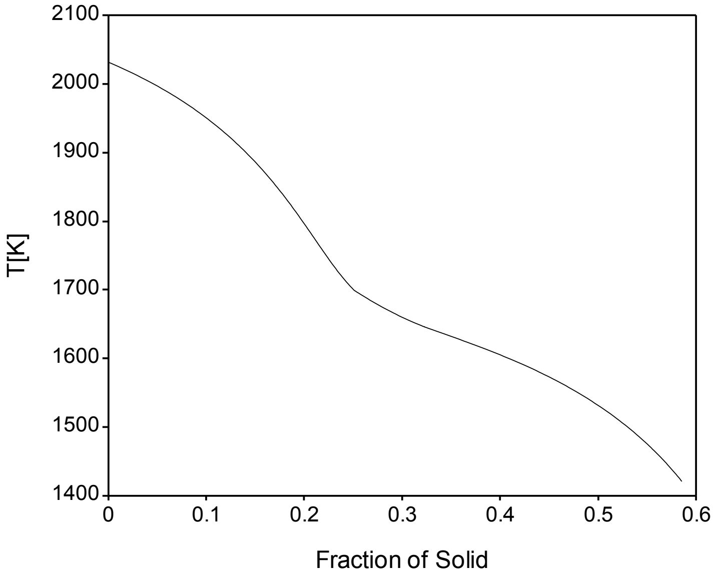

Figure 6.17 Solidification path for the alloy AN4-AC using Pandat database.

and the latter gives the solidification path shown in Figure 6.18.

The calculation of the solidification path using the Pandat database does not account for the formation of the T phase and the Cr_5Al_8 and Cr_4Al_9 aluminides, instead formation of Cr_3Si (A15 compound) is predicted. The calculation using ThermoCalc also does not account for the formation of the T silicide but predicts the formation of the Cr_5Al_8 and Cr_4Al_9 aluminides as well as many other intermetallic phases including Cr aluminides and Cr and Ti silicides. The failure of both databases to account for the formation of the T phase clearly demonstrates the weakness of the underlying phase equilibria data.

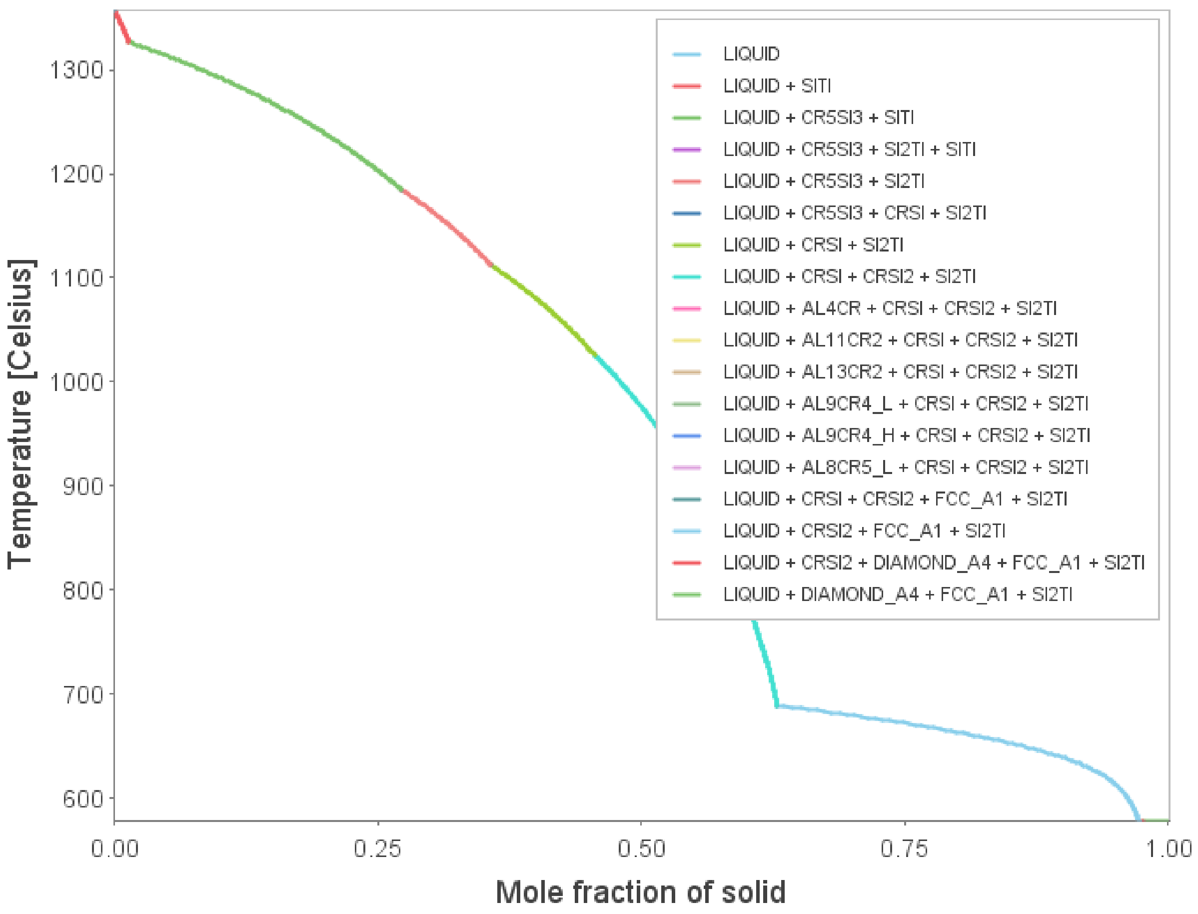

Figure 6.18 Solidification path for the alloy AN4-AC using ThermoCalc SSOL4 database

If we were to use the data in Du and Schuster [21], see section 6.3.1 above, and consider the actual Al+Si content in AN4-AC (see Table 6-3), which we consider as a Cr-Si-Ti alloy, then the primary phase should be the T phase. If the latter were to form first in the melt then the remaining liquid would become richer in Al and Cr and leaner in Si and Ti, in this melt the (**Cr**,Ti)$_5$(Si,Al)$_3$ would form with partitioning of Ti in (Cr,**Ti**)$_5$(Si,Al)$_3$ making the surrounding melt lean in Cr, Si and (probably) Ti and rich in Al and from this melt the two Cr aluminides would form with the sequence of their formation as indicated above by the melting temperatures of the unalloyed intermetallics. In other words, the suggested solidification path for AN4 is L → L + T → L + T + T1 → L + T + T1 + Cr_5Al_8 → T + T1 + Cr_5Al_8 + Cr_4Al_9.

The microstructure of AN4-HT1200 consisted of the T ($(Ti,Cr)_6Si_5$), T1 ($(Cr,Ti)_5(Si,Al)_3$) and $Cr_3(Si,Al)$ silicides and the $Cr_5(Si,Al)_8$ aluminide (Table 6-3) with changes in the fractions of all three phases compared with the cast alloy (Table 6-1), particularly for the T and T1 phases as the fraction of the former decreased significantly and the latter increased compared with the cast alloy owing to a phase transformation involving the formation of $Cr_3(Si,Al)$ in the microstructure, as indicated by the DSC data. There was no evidence regarding the presence of Cr(Si,Al) in AN4-HT1200. In the 1000 ^oC isothermal section of the Cr-Si-Ti system (the closest isothermal section to 1200 ^oC that is available in the literature, see Figure 2.16 (b) [21]) an alloy of composition Cr-50.4Si-4.6Ti (the actual composition of AN4-HT1200 when considering Al and Si together, see Table 6-3) falls in the $CrSi_2$-CrSi-T three phase field. If were to consider the same alloy in the Cr-Si-Al system (consider Cr and Ti together) then in the 1100 ^oC isothermal section in Liang et al. [40] the alloy falls close to the T1-$CrSi_2$-$Al_{58}Cr_{31}Si_{11}$ (τ_4 phase in Liang et al.[40]) or the T1-Cr_5Al_8- $Al_{58}Cr_{31}Si_{11}$ three phase fields.

The microstructure of AN4-HT1300 consisted of the T ($(Ti,Cr)_6Si_5$), T1 ($(Cr,Ti)_5(Si,Al)_3$) and $Cr_3(Si,Al)$ silicides and the $Cr_5(Si,Al)_8$ and $Cr_4(Al,Si)_9$ aluminides (Table 6-3) with changes in the fractions of all three phases compared with AN4-HT1200 (Table 6-1), particularly for the T and "normal" (i.e., not Ti rich) T1 phases as the fractions of both decreased significantly while the fraction of Ti rich Ti increased significantly compared with AN4-HT1200. The data would thus suggest a significant role for Ti at 1300 ^oC via its partitioning in the T1, in addition to a phase transformation involving the formation of $Cr_3(Si,Al)$ in the microstructure below 1200 ^oC, as indicated by the DSC data. There was no evidence regarding the presence of Cr(Si,Al) in AN4-HT1200. The above data for the heat treated alloy AN4 confirms (i) that the T phase is stabilised by the synergy of Cr and Ti (i.e., by transition metals, see section 5.3.1) with Al and Si, (ii) that Al controls (is important regarding) the stability of CrSi and $CrSi_2$ which it suppresses in favour of Cr_3Si, particularly when its (the Al) concentration in the alloy is high enough to lead to the formation of stable aluminide(s) with Cr. The data in Tables 6.1 and 6.3 also points to a key role played by Ti as the microstructure approaches equilibrium.

6.3.3 Mechanism of oxidation in multiphase Cr-Si-Al-Ti alloy

The oxides were characterized using EDX analysis and elemental maps. An important factor in the oxidation of the alloys would be any depletion of the Al, Cr and Ti below the scale that would lead to phase transformations in the substrate below the scale during oxidation. This would require the study of cross sections of the oxidized specimens. The scale characterization using glancing angle XRD (GAXRD) at different incident angles could not give us reliable information about the phases being present beneath the scale.

The most important observation from the oxidation of the alloys AN3 and AN4 at 800, 1000 and 1200 °C is that the alloys did not show any sign of accelerated or pest oxidation, as was the case for the alloys AN1 and AN2. Furthermore, the alloys AN3 and AN4 gained a small amount of weight and formed either a mixture of oxides or a continuous scale, see Table 6-6. According to available phase equilibria data for the Cr-Si-O ternary system by Matskevich et al. [125] and the Ti-Si-O ternary system by Shalaeva et al. [137], the Cr silicides are in equilibrium with silica at 1000 °C (Figure 6.19) whereas at 1023 °C the Ti_5Si_4 and Ti_3Si silicides are not in equilibrium with a single oxide and Ti_5Si_3 can be in equilibrium with Ti oxide and SiO_2 and only TiSi and $TiSi_2$ can be in equilibrium with silica. However, there is disagreement about Cr silicides, as Grabke et al. [88] reported that $CrSi_2$ formed Cr_2O_3 in the temperature range 900 to 1050 °C despite of the fact that the Cr activity is lower than the Si activity.

Table 6-6 Summary of the scales formed on the alloys AN3 and AN4 after isothermal oxidation at 800, 1000 and 1200 °C in air

Alloy	Temperatures		
	800 °C	1000 °C	1200 °C
Cr-45Si-5Al-5Ti (AN3)	Whiskers SiO_2, Al_2O_3, Cr_2O_3, TiO_2, Mullite No spallation	Cells/whiskers SiO_2, Al_2O_3, Cr_2O_3, TiO_2, Mullite No spallation	Continuous scale Al_2O_3 Spalled
Cr-25Si-25Al-5Ti (AN4)	Whiskers SiO_2, Al_2O_3, Cr_2O_3, Mullite No spallation	Cell Al_2O_3 Continuous scale Spalled	Buckeled scale $(Al,Cr)_2O_3$, Mullite Partially Spalled in ridges

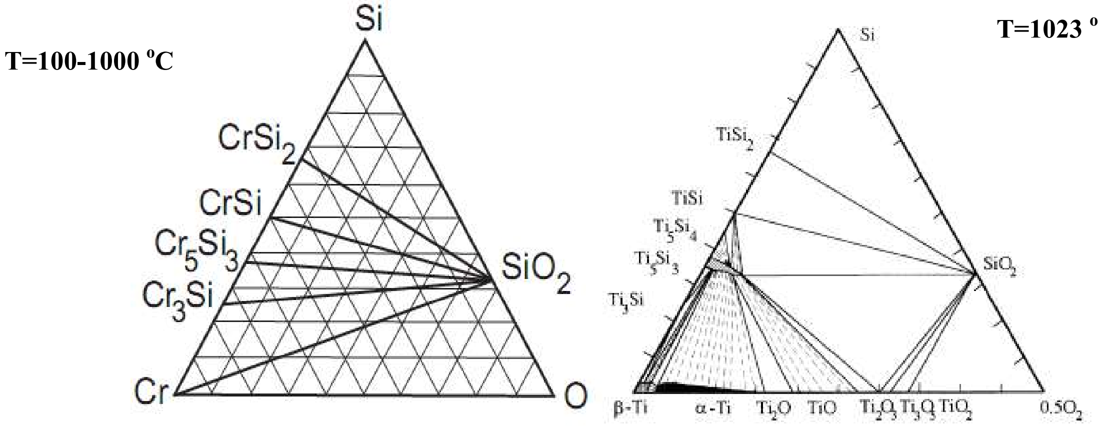

(a) (b)

Figure 6.19 Ternary phase diagrams of the (a) Cr-Si-O [125] and (b) Ti-Si-O [137] systems.

However, the Si activity in the $CrSi_2$ formed in the alloy AN3 is not comparable to that of reported by Grabke et al. because of solubility of Al up to about 15 % in $CrSi_2$ in the alloy AN3 that can cause a change in the activity of Cr accordingly. As reported earlier, the microstructure of the alloy AN3 consisted of the $(Ti,Cr)_6Si_5$, $(Cr,Ti)_5(Si,Al)_3$ and $Cr(Si,Al)_2$ intermetallics and was stable in the temperature range 800 to1200 °C. According to the data obtained from the EDX analyses of the scales (Figures 6.20, 6.21, 6.22) and the glancing angle XRD of oxidized specimens, which was shown in Figure 6.12, mixture of oxides was formed on the surface of the alloy AN3 at 800 and 1000 °C and a continuous alumina scale at 1200 °C that was partially spalled and crack had propagated on the surface of the scale (Figure 6.7 plot 3 and Figure 6.10 c1/c2). The spallation of the scale was attributed to the thermal expansion mismatch between the alloy and alumina scale and the presence of the pores (see Figure 6.10 c2 and c5) that decreased the adhesion of the alumina scale to the substrate. The oxidation of the alloy at 1200 °C showed that the alloy lost weight after (t>10 hours), see Figure 6.7 which may be attributed toCr_2O_3 volatilization due to the exposure of the substrate during the isothermal oxidation at 1200 °C. In this regard, subsurface depletion of Al driven by selective oxidation to form the alumina scale triggers phase transformation in the alloy just below the evolving oxide scale to less oxidation-resistant intermetallic phases which can prevent the re-formation of the spalled scale.

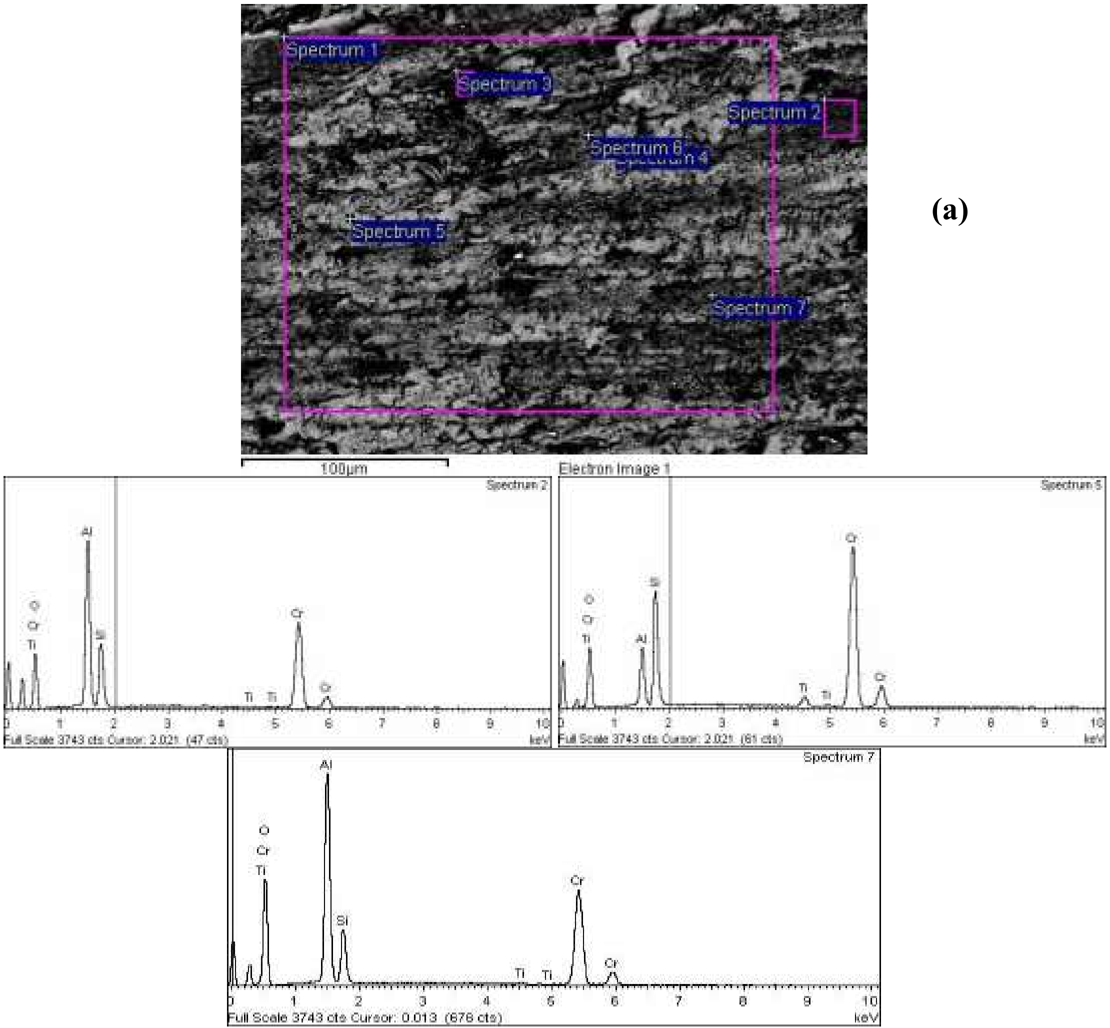

Spectrum 1
Spectrum 3
Spectrum 2
Spectrum 6
Spectrum 4
Spectrum 5
Spectrum 7
100µm
Electron Image 1
Spectrum 2
Al
O
Cr
Ti
Si
Ti
Ti
Cr
Cr
0 1 2 3 4 5 6 7 8 9 10
keV
Full Scale 3743 cts Cursor: 2.021 (47 cts)
Spectrum 5
Cr
Si
O
Cr
Ti
Al
Ti
Ti
Cr
0 1 2 3 4 5 6 7 8 9 10
keV
Full Scale 3743 cts Cursor: 2.021 (61 cts)
Spectrum 7
Al
O
Cr
Ti
Si
Ti
Ti
Cr
Cr
0 1 2 3 4 5 6 7 8 9 10
keV
Full Scale 3743 cts Cursor: 0.013 (676 cts)

(a)

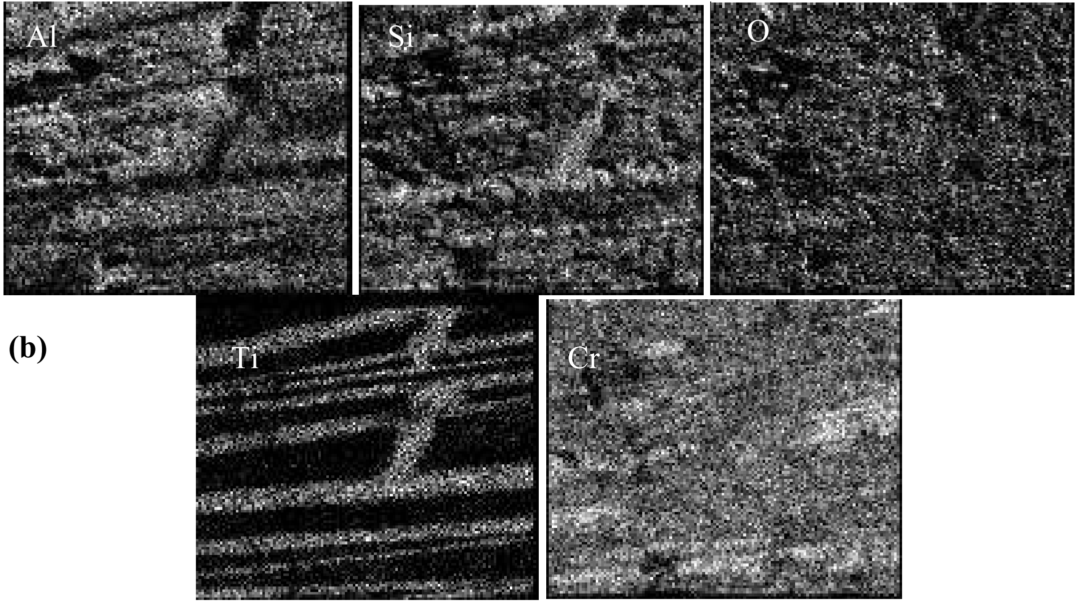

Al
Si
O
Ti
Cr

(b)

(c)

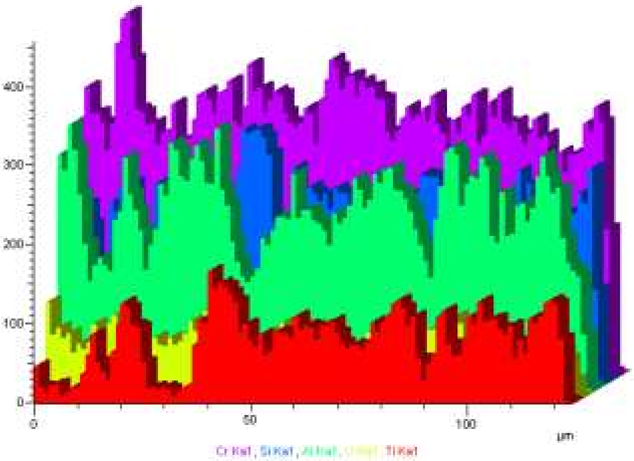

Figure 6.20 a) Surface SEM-BSE image of oxidized AN3 specimen at 800 ^{o}C with EDX spectra taken for indicated areas and/or spots b) surface elemental maps of Al, Si, Cr, Ti and O from the indicated area c) line scan of the oxidized specimen at 800 ^{o}C.

(a)

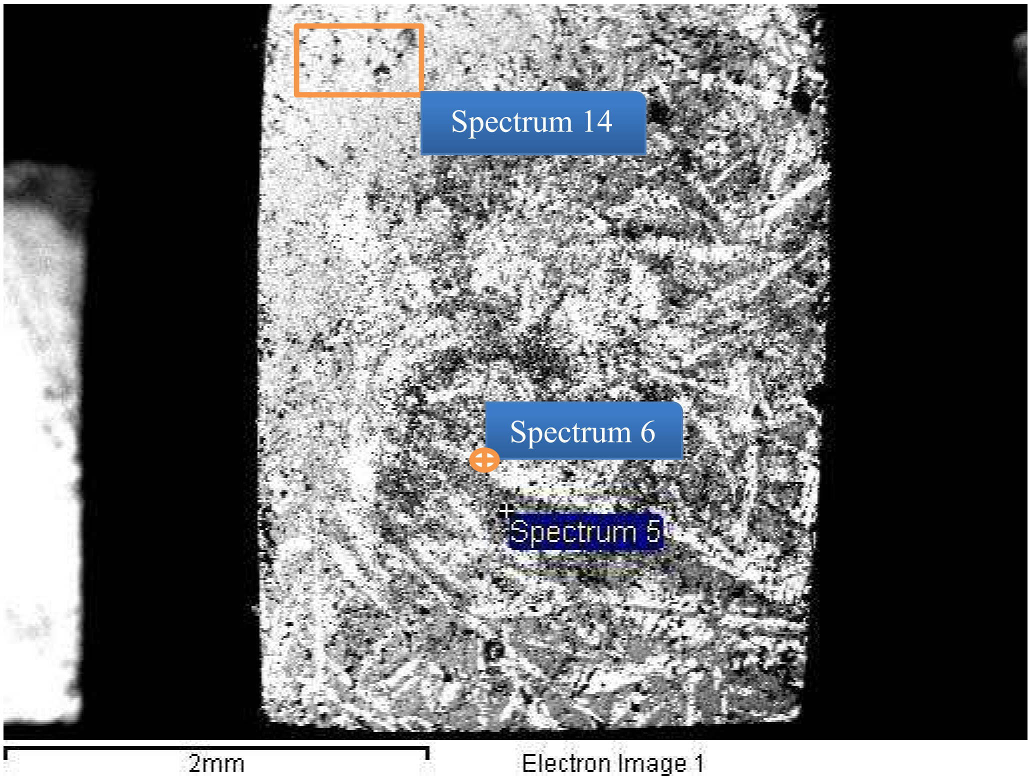

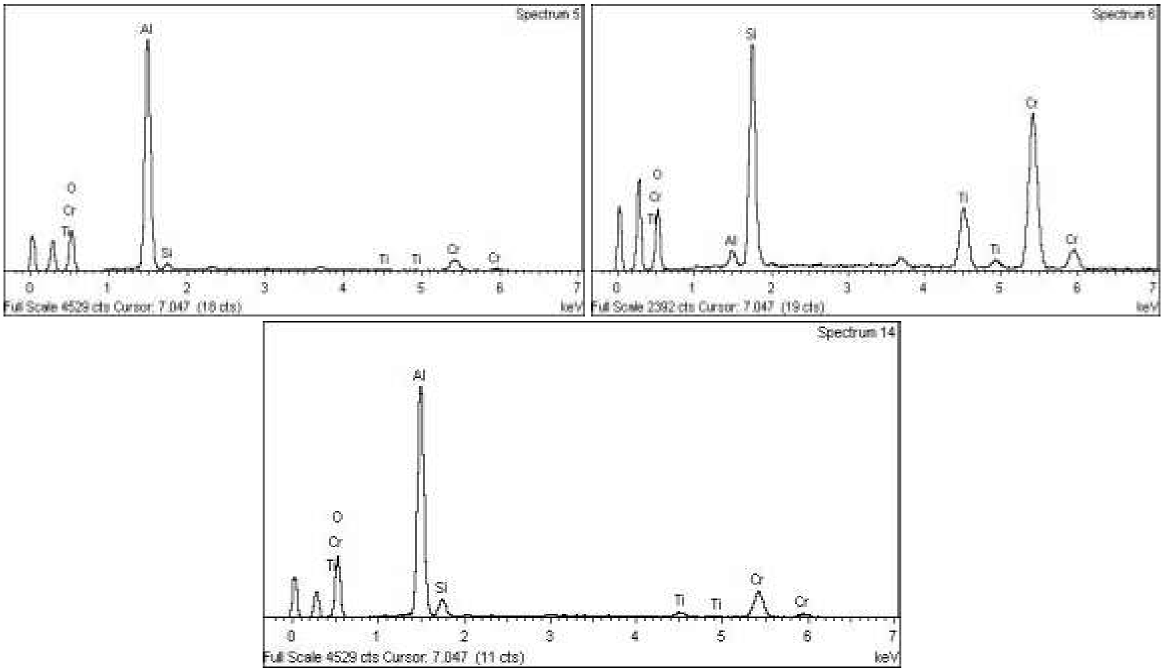
Spectrum 5
Al
O
Cr
Ti
Si
Ti
Ti
Cr
Cr
0 1 2 3 4 5 6 7
Full Scale 4529 cts Cursor: 7.047 (16 cts)
keV
Spectrum 6
Si
Cr
O
Cr
Ti
Al
Ti
Ti
Cr
0 1 2 3 4 5 6 7
Full Scale 2392 cts Cursor: 7.047 (19 cts)
keV
Spectrum 14
Al
O
Cr
Ti
Si
Ti
Ti
Cr
Cr
0 1 2 3 4 5 6 7
Full Scale 4529 cts Cursor: 7.047 (11 cts)
keV

(b)

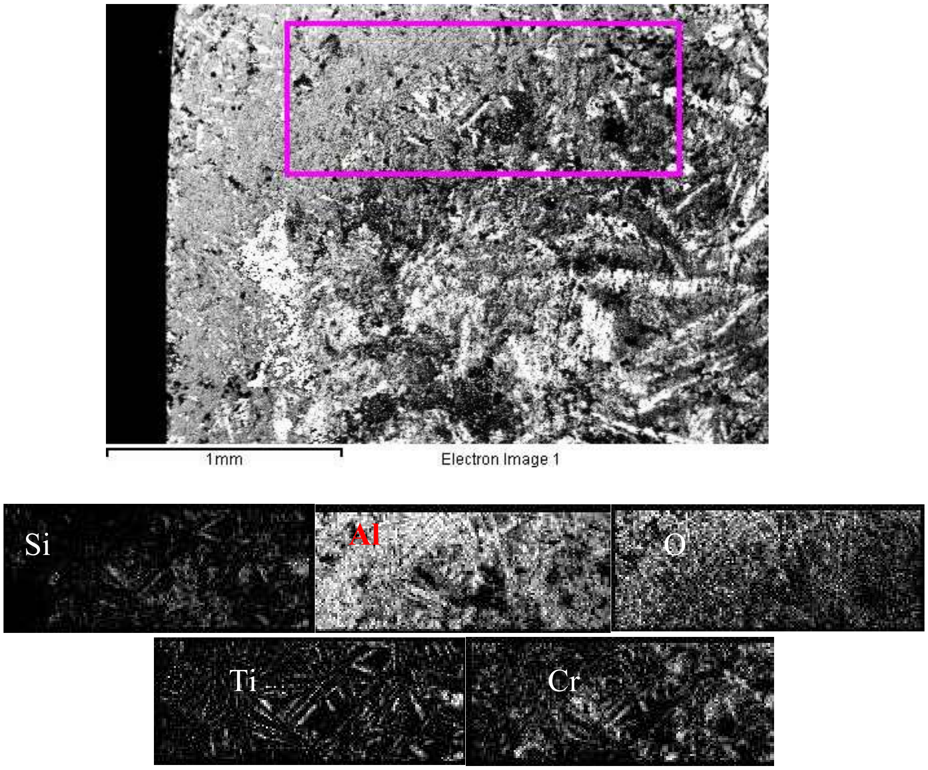
1mm
Electron Image 1
Si
Al
O
Ti
Cr

(c)

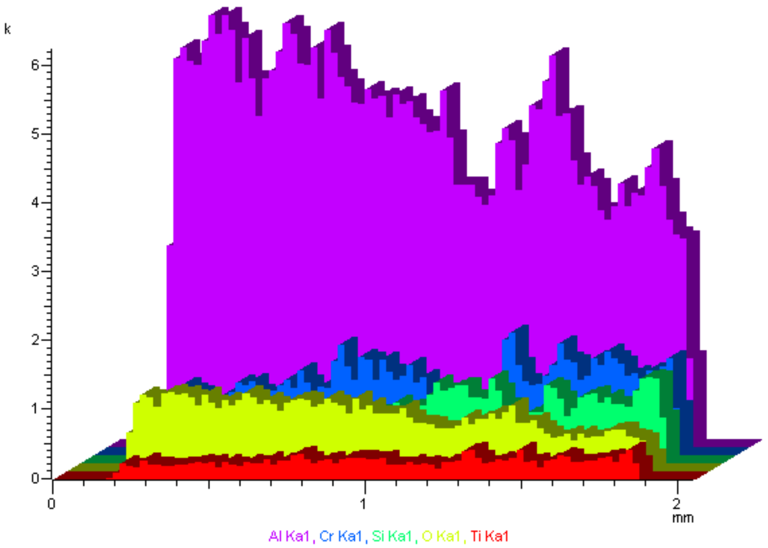

Figure 6.21 Surface SEM-BSE image of oxidized AN3 specimen at 1000 °C with EDX spectra taken for the indicated areas and/or spots b) surface elemental maps of Al, Si, Cr, Ti and O from the indicated area c) line scan of the oxidized specimen at 1000 °C.

During oxidation at 800 °C mixture of oxides (composite scale) formed on the surface (Table 6-6) where different oxide formed on the different precursors owing to the different Al, Si, Cr, and Ti activity in each precursor and the different oxygen diffusion rate. For instance, the compositions of the oxides that formed the scale on the Cr $(Si,Al)_2$ phase were 43, 32, 24 and 1 % wt., respectively for alumina, silica, chromia and titania and for the $(Ti,Cr)_6Si_5$ the compositions of the oxides were 1, 10.6, 76.4 and 11.2 % wt., respectively for alumina, silica, chromia and titania. The composite scale formed on the $(Cr,Ti)_5(Si,Al)_3$ silicide consisted of 9, 46, 43 and 2.5 %wt. respectively of alumina, silica chromia and titania. According to binary phase equilibria for the Cr_2O_3-SiO_2, Cr_2O_3-Al_2O_3 and SiO_2-Al_2O_3 oxide systems (Figure 6.23) at 800 °C the oxides are not miscible and soluble in one another except in Al_2O_3-SiO_2 where mullite (solid solution of alumina and silica) is formed. Therefore by ignoring the negligible amount of TiO_2 in the composite scale formed on the $Cr(Si,Al)_2$ precursor, at 800 °C the scale contained 60% mullite, 15 % silica and 25 % chromia, calculated according to the Cr_2O_3-SiO_2-Al_2O_3 system in Figure 6.23. Similarly, the scale formed on the $(Cr,Ti)_5(Si,Al)_3$ precursor contained 10% mullite, 36 % silica and 45.8 % Cr_2O_3+TiO_2.

The scale formed on the alloy AN3 at 1000 °C, similarly to that formed at 800 °C, was a composite scale formed on the different constituents of the alloy (Table 6-6). The composition of

(a)

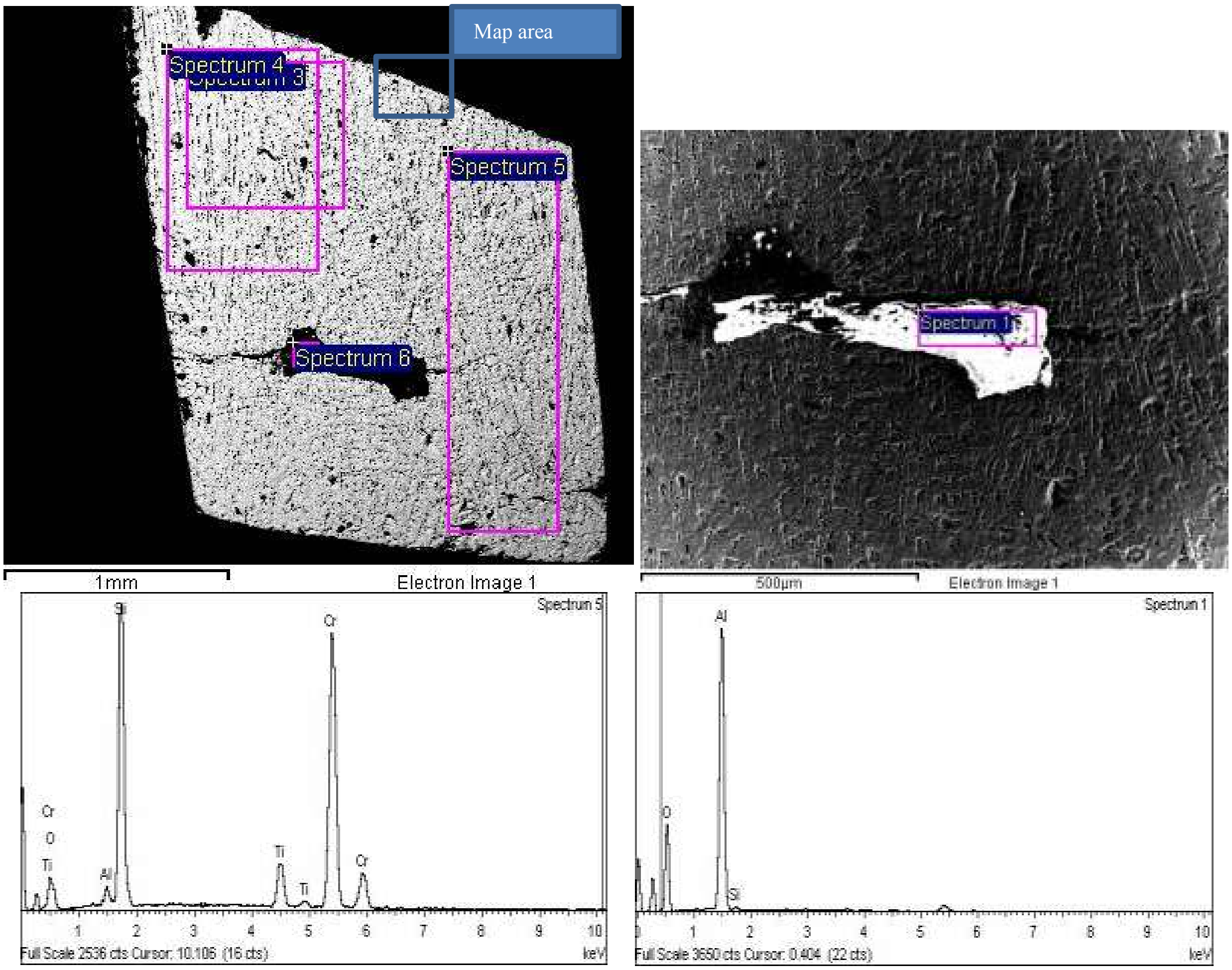
Map area
Spectrum 4
Spectrum 3
Spectrum 5
Spectrum 6
1mm
Electron Image 1
Spectrum 1
500µm
Electron Image 1
Spectrum 5
Si
Cr
Cr
O
Ti
Al
Ti
Ti
Cr
1
2
3
4
5
6
7
8
9
10
Full Scale 2536 cts Cursor: 10.106 (16 cts)
keV
Spectrum 1
Al
O
Si
0
1
2
3
4
5
6
7
8
9
10
Full Scale 3650 cts Cursor: 0.404 (22 cts)
keV

(b)

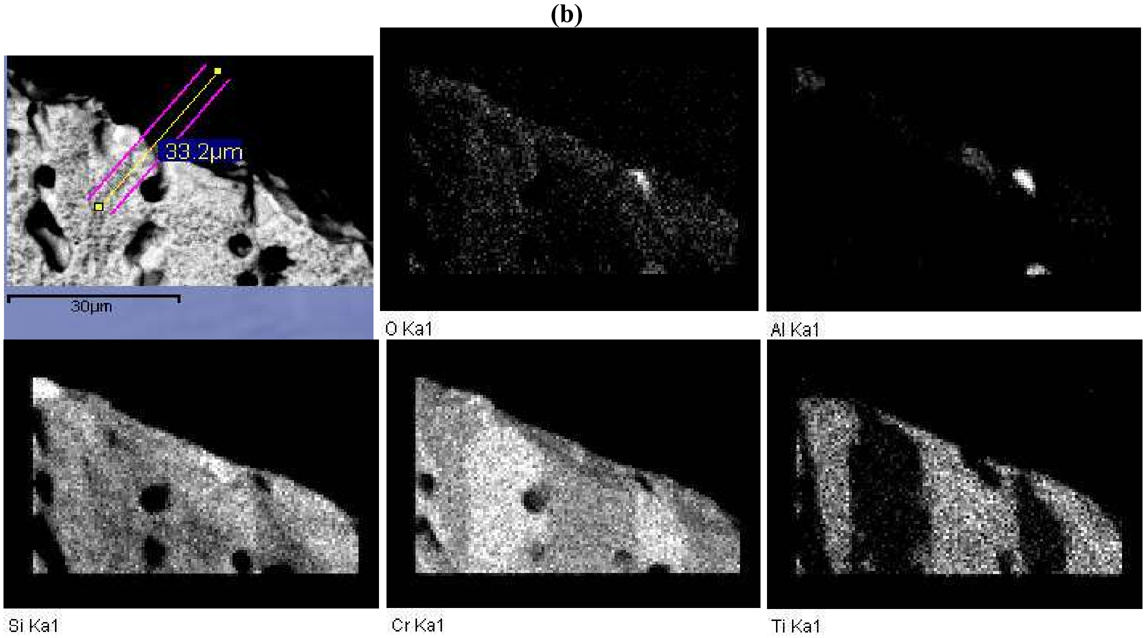
33.2µm
30µm
O Ka1
Al Ka1
Si Ka1
Cr Ka1
Ti Ka1

(c)

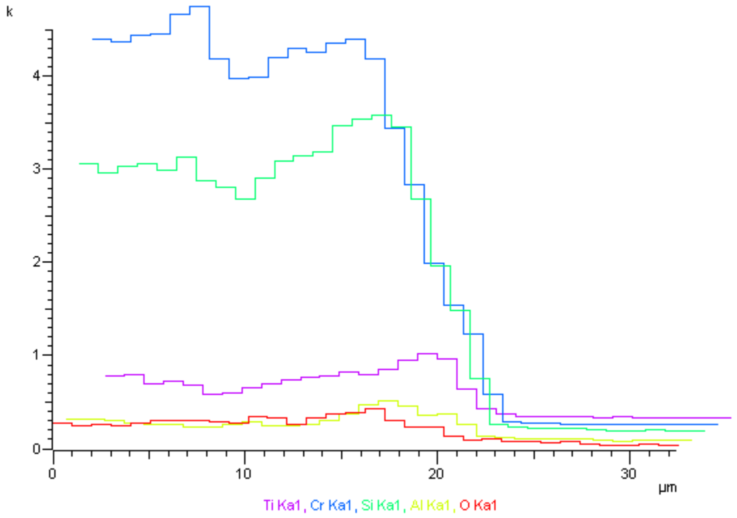

Figure 6.22 Surface SEM-BSE image of oxidized AN3 specimen at 1200 °C b) surface elemental maps of Al, Si, Cr, Ti and O from the indicated area c) line scan of the oxidized specimen at 1200 °C as indicated in (b).

the scale formed on the $Cr(Si,Al)_2 + Cr_5Si_3$ precursor after oxidation at 1000 °C for 100 hours was 91, 5 and 4 wt. % alumina, silica and chromia respectively, and according to the Cr_2O_3-SiO_2-Al_2O_3 system consisted of mullite, alumina and chromia with percentages 16.3%, 79.7% and 4%, respectively. The composite scale formed on the Ti_6Si_5 at 1000 °C consisted of chromia, silica and titania. Figure 6.10 (b) shows that there was scale spallation on the Ti_6Si_5 and that beneath the scale there was a high volume fraction of pores. In the ternary Cr_2O_3-SiO_2-Al_2O_3 system, the composition of the composite scale formed on Ti_6Si_5 is placed on the right hand side of the ternary (Figure 6.23) where the alumina content is almost negligible and the TiO_2 has no solubility either in the Cr_2O_3 or SiO_2 (at 1000 °C [138]), therefore the scale formed as a mixture of corundum and silica that subsequently spalled.

During oxidation at 1200 °C single phase alumina oxide formed on the surface but the scale suffered from partial spallation due to its weak adhesion to the substrate. Subsurface depletion of aluminium driven by selective oxidation to form the alumina scale could cause a disruption in the formation of continuous scale.

From a phenomenological standpoint, in the oxidation of a multi-phase alloy (a) a single-phase reaction product can form from the cooperative reaction of the phases or (b) a composite reaction product can form when the phases react independently. In cooperative oxidation, the Al, Si or Cr rich second and third phases maintain the growth of the protective scale whereas in the independent mode of multiphase oxidation all the constituents participate in the oxidation and a composite scale rather than an exclusive continuous layer of the scale, is formed. The oxidation behaviour of the alloy AN3 at 800 and 1000 ^{o}C conformed to the independent mode of oxidation whereas at 1200 ^{o}C, the alloy exhibited cooperative oxidation and formed a single phase continuous scale despite scale adhesion issues.

The microstructure of the alloy AN4 consisted of the $(Ti,Cr)_6Si_5$, $(Cr,Ti)_5(Si,Al)_3$, Cr_5Al_8 and Cr_4Al_9 intermetallics with the sum of the volume fractions of aluminides and silicides being respectively 42.4 % and 57.6 % (Table 6-1). Unlike the alloy AN3, in AN4 there were aluminides rich in Si in the microstructure and the activity of the Al was increased due to high vol. % of aluminide precursors. However, the concern of phase transformation(s) below the scale was seen for this alloy as aluminium depletion below the evolving scale would lead to the formation of any lower Al-containing intermetallic phases, and prevent the formation of a continuous scale and/or the repair of the spallation.

(a)

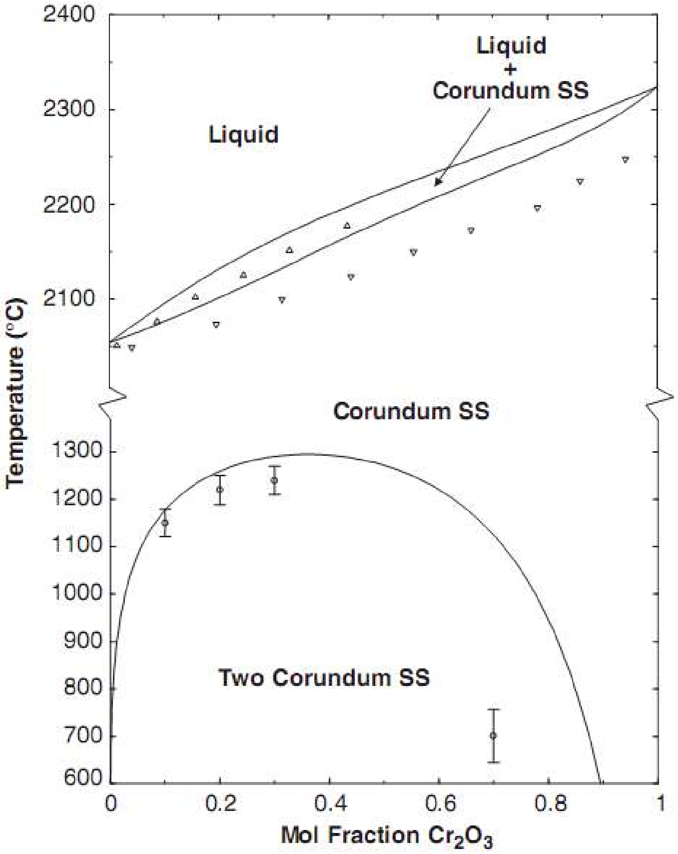
Liquid
+
Corundum SS
Liquid
Corundum SS
Two Corundum SS
Temperature (°C)
2400
2300
2200
2100
1300
1200
1100
1000
900
800
700
600
0
0.2
0.4
0.6
0.8
1
Mol Fraction Cr_2O_3

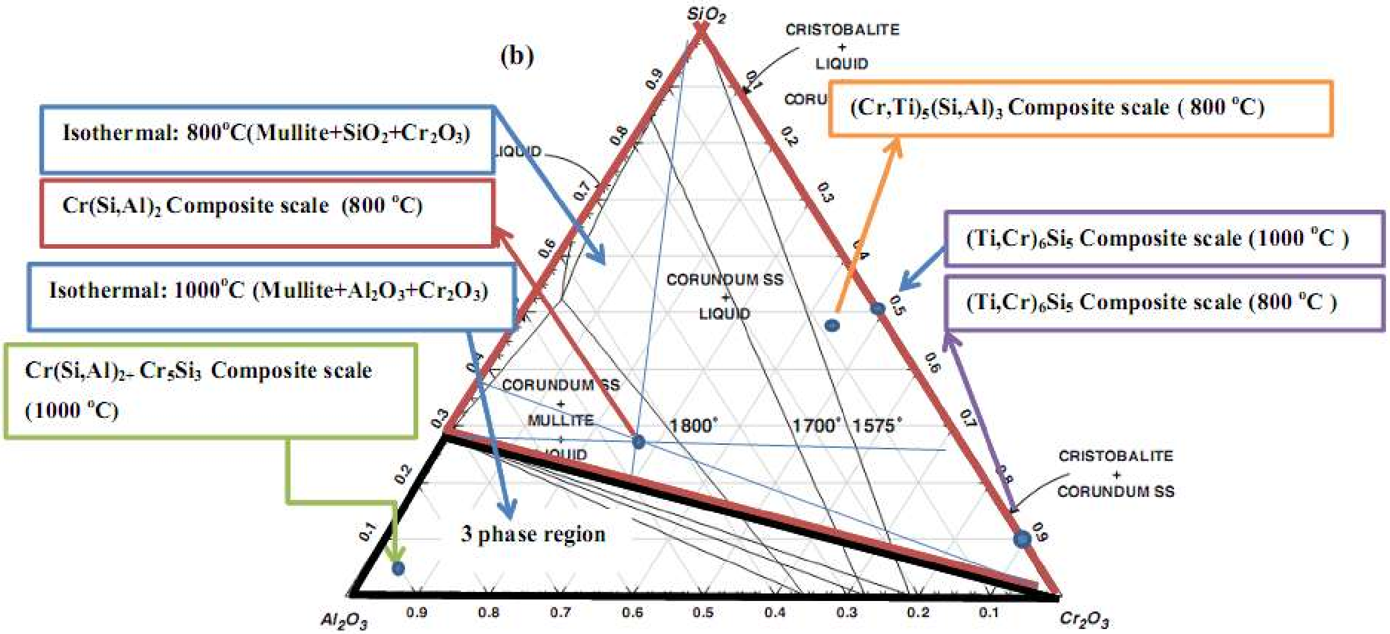

Figure 6.23 Computed Al_2O_3-Cr_2O_3 system phase diagram with the experimental solidus (▽) and liquidus (Δ) values of Bunting and the miscibility gap determination of Sitte (O)(a) ,computed ternary phase diagram for the Al_2O_3-Cr_2O_3-SiO_2 indicating isothermal at 1575,1700,and1800 °C (composition is given in mass fraction to allow comparison with published diagram) (b) [127]

(a)

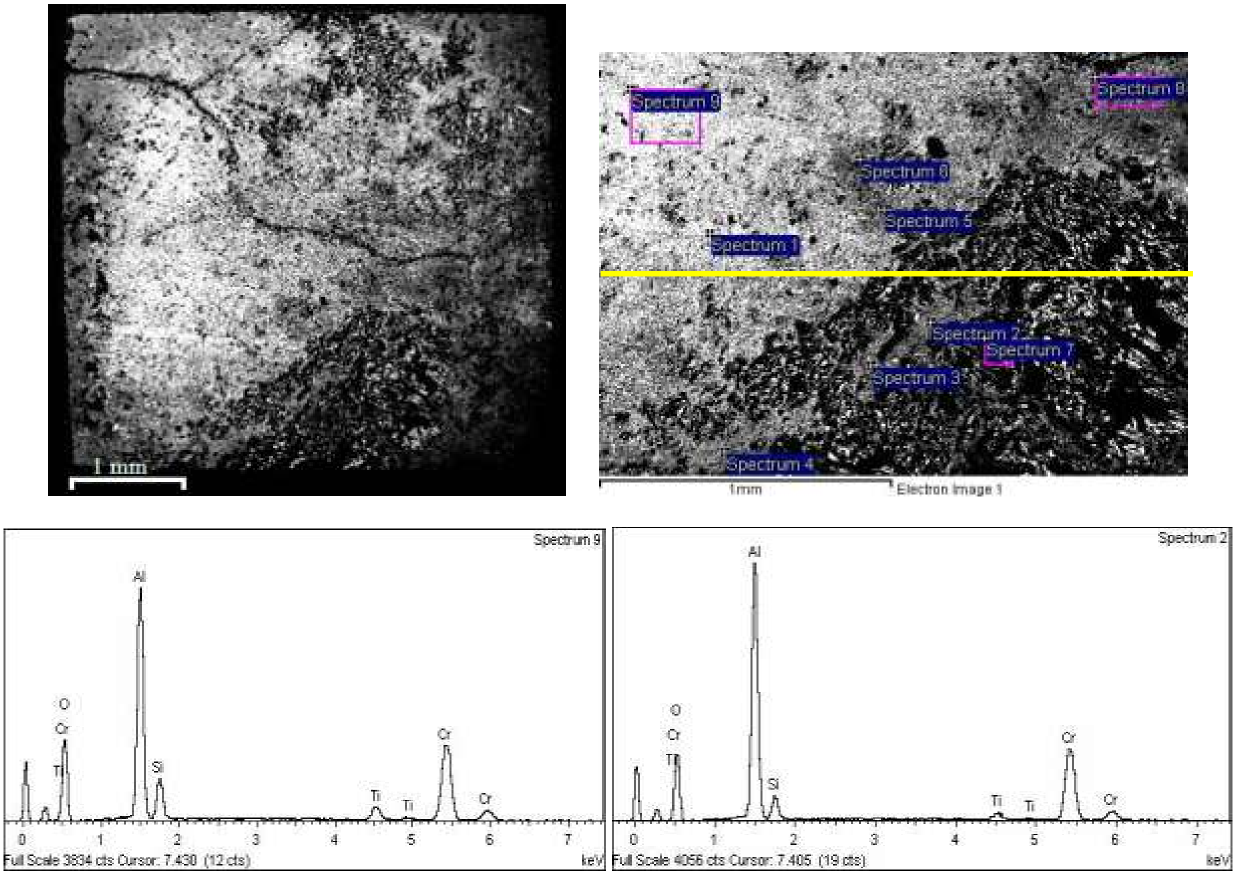

(b)

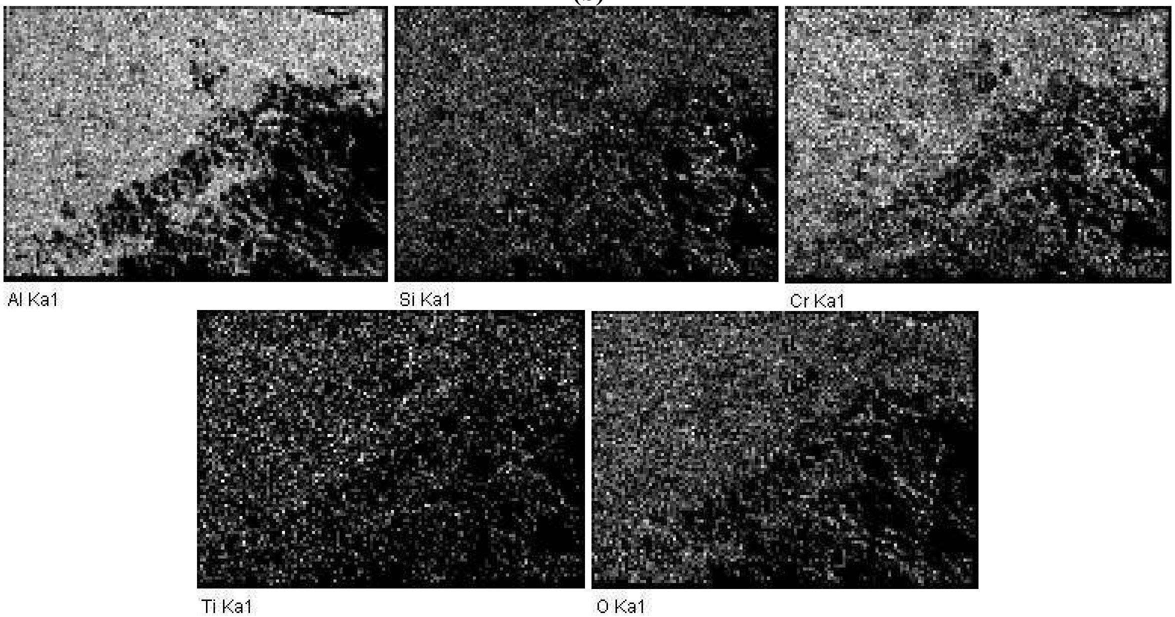

Al Ka1 Si Ka1 Cr Ka1

Ti Ka1 O Ka1

(c)

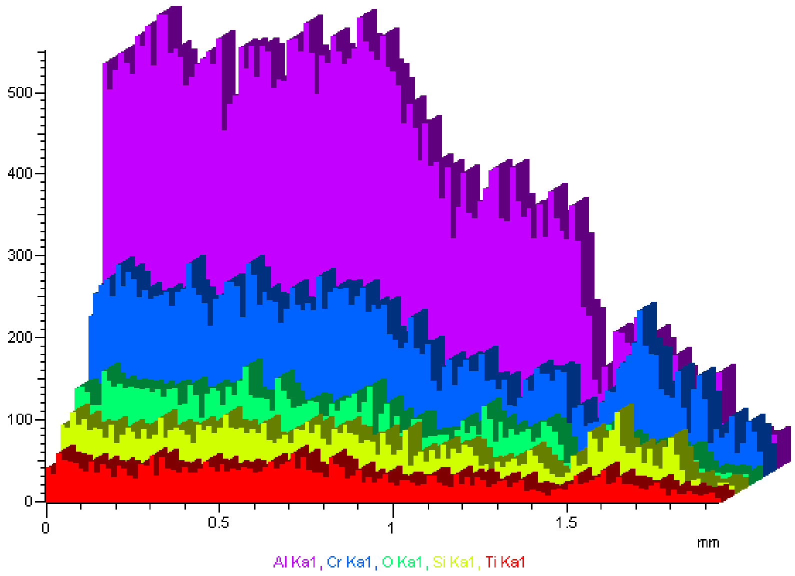

Figure 6.24 a) Surface SEM-BSE image of oxidized AN4 specimen at 800 °C with EDX spectra from the indicated area and/or spots b) surface elemental maps of Al, Si, Cr, Ti and O from indicated area c) line scan of the oxidized specimen at 800 °C as indicated in (a) with yellow line.

According to the EDX data (Figures 6.24, 6.25, 6.26) and the glancing angle XRD (Figure 6.13), the alloy AN4 at 800 °C, formed a continuous scale that consisted of mullite, alumina and chromia with composition 87, 8 and 5 wt.%. respectively of Al_2O_3, Cr_2O_3 and SiO_2. In the Al_2O_3-Cr_2O_3-SiO_2 ternary system shown in Figure 6.23 b, the scale composition lies in the 3 phase region of mullite, alumina and chromia. It was concluded that in the alloy AN4 its precursor phases had acted cooperatively to form a composite scale. The composition of the scale formed on AN4 at 800 °C was very much close to that formed on the alloy AN3 at 1000 °C. The % volume of alumina, mullite and chromia in the composite scale formed on the alloy AN4 at 800 °C were 50, 42, and 8 vol.% respectively.

Unlike the composite scale formed on the alloy AN4 at 800 °C, at 1000 °C a single continuous alumina scale was formed that spalled off during oxidation. The oxidation of the AN4 alloy at 1200 °C was affected by the phase transformation that occurred in the alloy at 1200 °C. During oxidation at 1200 °C the alloy was confronted by two different phase transformations, one driven by phase equilibria in the bulk and the other by the Al depletion beneath the scale both of which

(a)

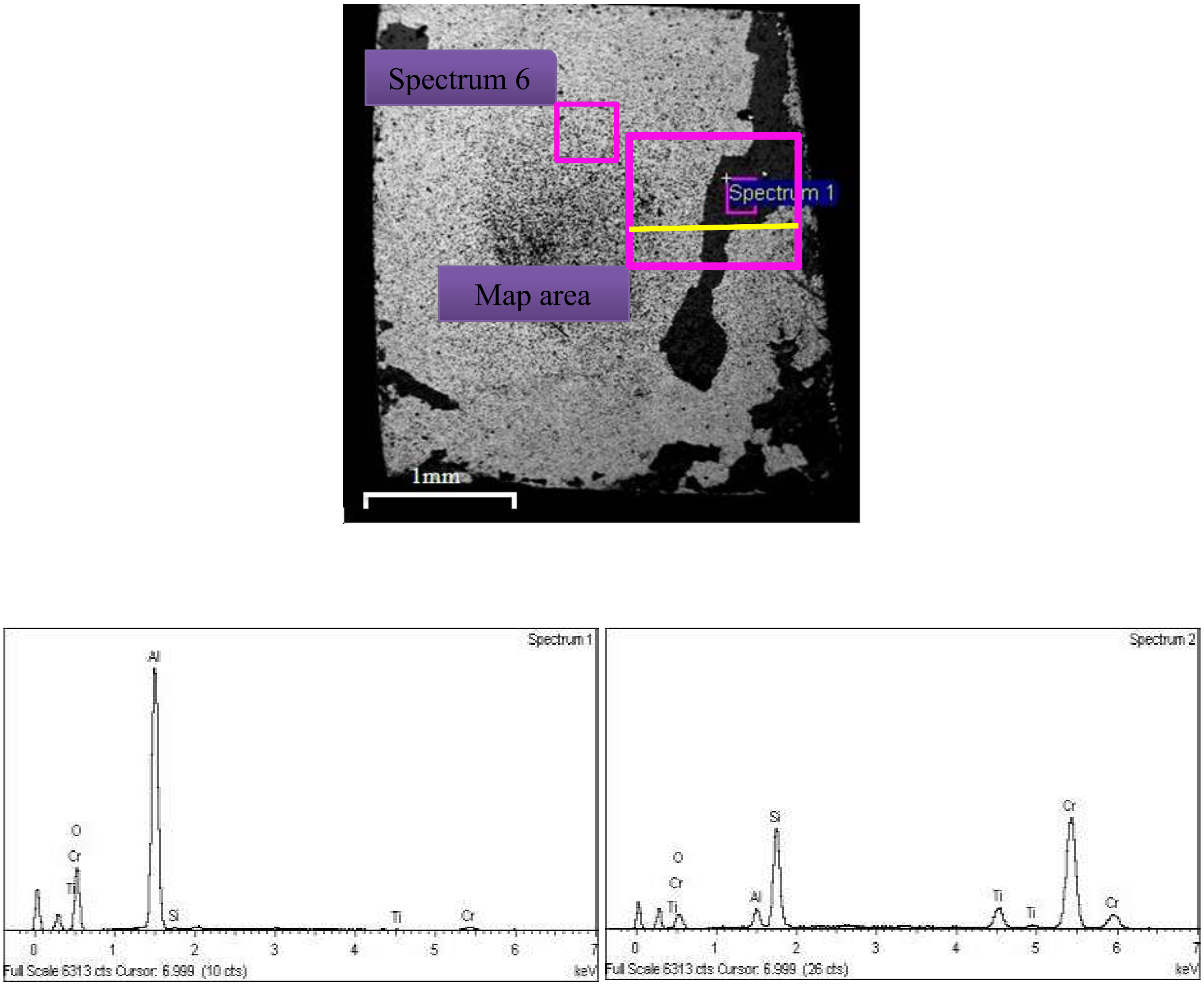
Spectrum 6
Map area
Spectrum 1
1mm
Spectrum 1
Al
O
Cr
Ti
Si
Ti
Cr
Full Scale 6313 cts Cursor: 6.999 (10 cts)
keV
Spectrum 2
Si
Cr
O
Cr
Ti
Al
Ti
Ti
Cr
Full Scale 6313 cts Cursor: 6.999 (26 cts)
keV
0
1
2
3
4
5
6
7

(b)

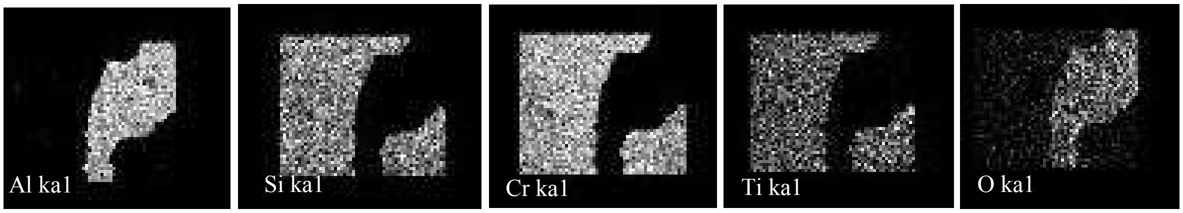
Al ka1
Si ka1
Cr ka1
Ti ka1
O ka1

(c)

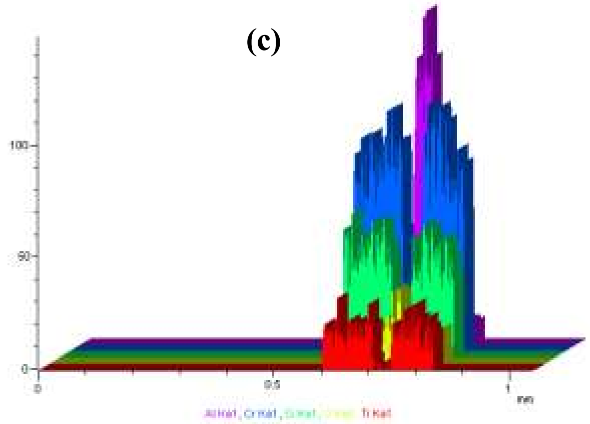

Figure 6.25 Surface SEM-BSE image of oxidized AN4 specimen at 1000 ^{o}C with EDX spectra from the indicated areas and/or spots b) surface elemental maps of Al, Si, Cr, Ti and O from indicated area c) line scan (yellow line) of the oxidized specimen at 1000 ^{o}C.

(a)

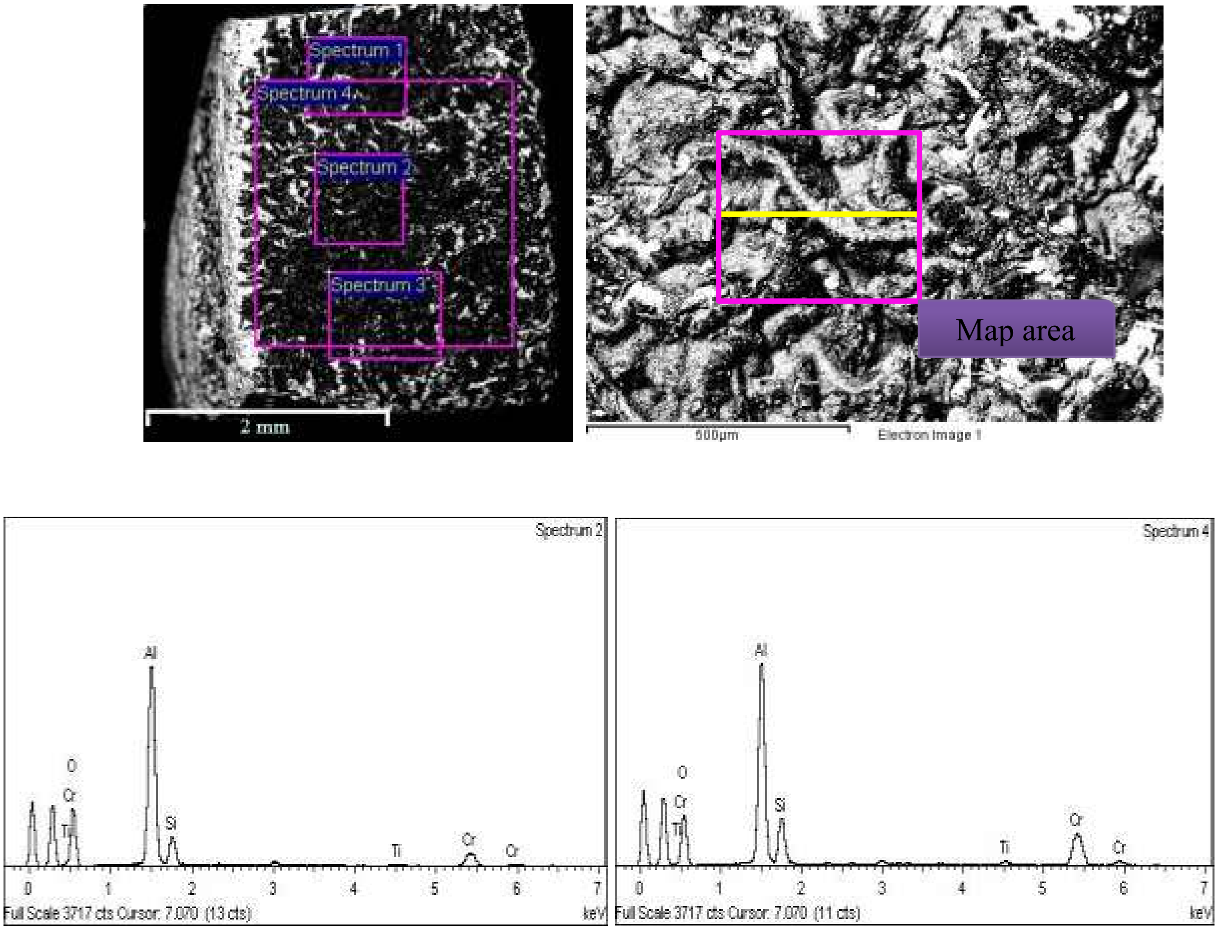

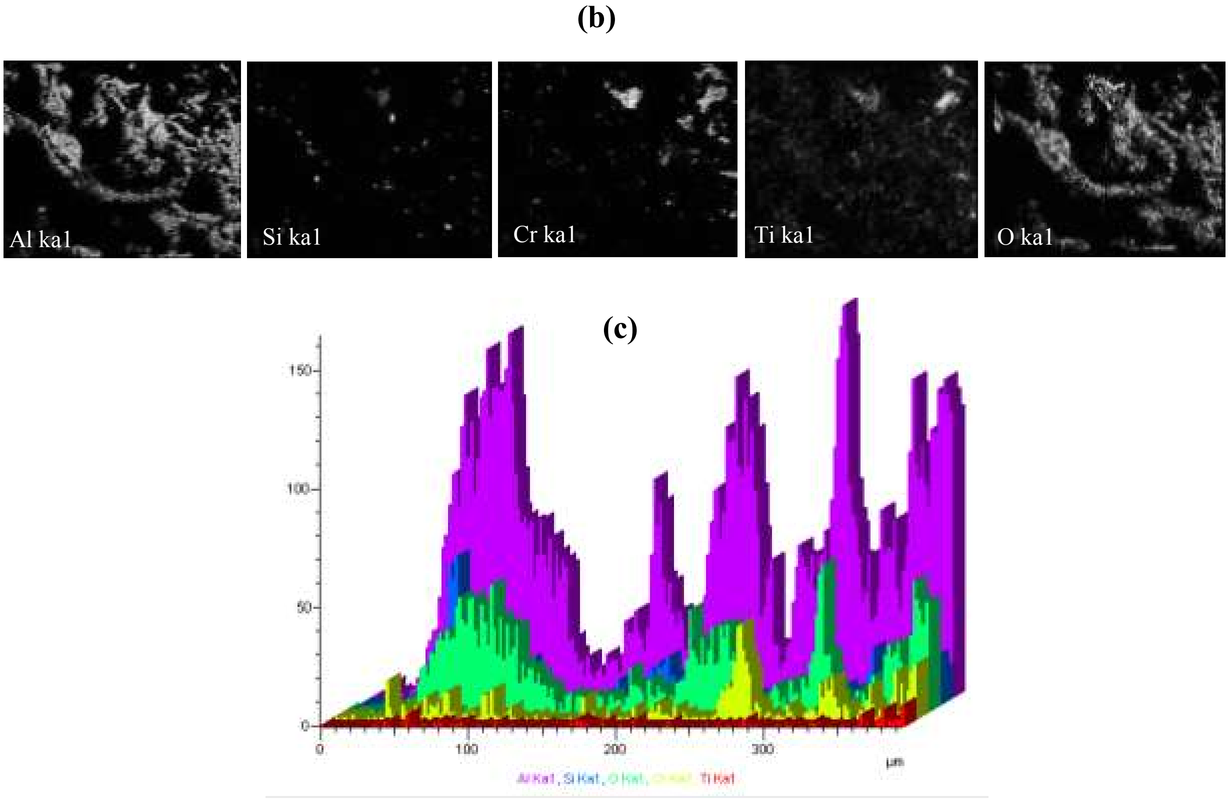

Figure 6.26 Surface SEM-BSE image of oxidized AN4 specimen at 1200 °C with EDX spectra from the indicated areas and/or spots b) surface elemental maps of Al, Si, Cr, Ti and O from indicated area c) line scan (yellow line) of the oxidized specimen at 1200 °C.

resulted to changes in the volume fractions of phases and phase types. Indeed, in AN4-HT1200, the volume fraction of Ti_6Si_5 decreased and the volume fractions of Al_8Cr_5 and Cr_5Si_3 increased. The increase in the vol.% of the aluminide meant that more Al was available to form the scale and the increase of the vol.% of Cr_5Si_3 meant that silica formation was more likely (easier). Thus, the scale formed on the alloy AN4 at 1200 °C was mostly corundum solid solution $(Al,Cr)_2O_3$ and mullite that formed in some area in the ridges where the corundum had spalled.

The alloys AN3 and AN4 exhibited parabolic or near parabolic oxidation behaviour for the whole oxidation time with relatively low oxidation rate constants (kp) with the exception of AN3 at 1200 °C where the parabolic behaviour was followed by paralinear oxidation after 16 hours. The paralinear behaviour after 16 hours. was attributed to formation of alumina scale and volatilization of Cr (parabolic weight gain plus a linear weight loss). The weight gain of the alloy

AN3 was 0.11 mg/cm^2 at 800 ^oC followed by an increase to 0.39 mg/cm^2 at 1000 ^oC and to 0.74 mg/cm^2 at 1200 ^oC (parabolic section). The weight gain of the alloy AN4 was 0.52, 1.43 and 1.86 mg/cm^2 respectively for 800, 1000 and 1200 ^oC.

In order to correlate alloy composition to oxidation rates, data obtained from this study is plotted in Figure 6.27 with data for Ni, Fe, or Pt based intermetallics. The alloy AN3 and AN4 are among those intermetallics that form alumina scale following parabolic oxidation behaviour and have oxidation rate constants (kp) between 6x10^{-12} g/cm^{4}s and 5x10^{-11} g/cm^{4}s at 1200 ^oC. Despite the fact that the alloy AN4 had high volume fraction of aluminium rich intermetallics (Al_8Cr_5 and Al_9Cr_4), the alloy had relatively poor oxidation resistance compared with the other alloys in Figure 6.27. It is suggested that the poor oxidation behaviour of AN4 was due to the high oxygen solubility in Ti-rich precursor phases since high oxygen permeability can be highly disruptive regarding the ability to establish continuous protective scale [57]. This could be occurred due to formation of internal oxidation and also by increasing the thickness of the scale which is not desirable.

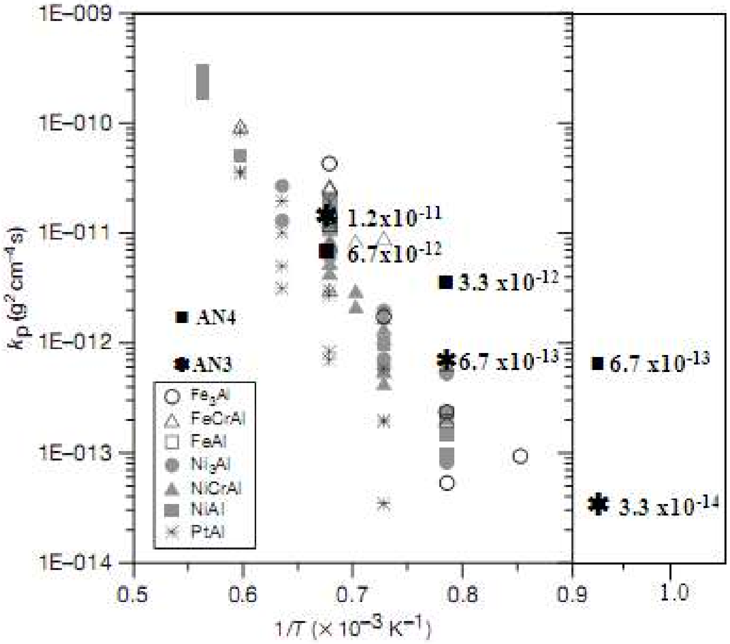

Figure 6.27 Parabolic rate constants showing the Al_2O_3 scale growth rate on different Fe, Ni, and Pt-based alloys. The results of the present study are marked by bold star (AN3) and solid square (AN4) [61].

The oxidation rate constants of the alloy AN3 and AN4 are plotted together with those of chromia, silica and alumina forming alloys in Figure 6.28. At 800 ^{o}C, the alloy AN3 is placed inside the alumina zone whereas the alloy AN4 is placed in the area between alumina and chromia forming alloys and close to the lower band of chromia forming alloys. At 1000 ^{o}C, the alloy AN3 is still in the alumina zone and the alloy AN4 is close to the alumina/chromia interface. At 1200 ^{o}C, the alloy AN3 is still in the alumina band and the alloy AN4 move to the zone where the alumina forming alloys are stable. Compared with the results of Zamoum et al. [129], the oxidation rate constants of the alloy AN3 and AN4 at 1200 ^{o}C are almost equal to that of M_7Si_6.

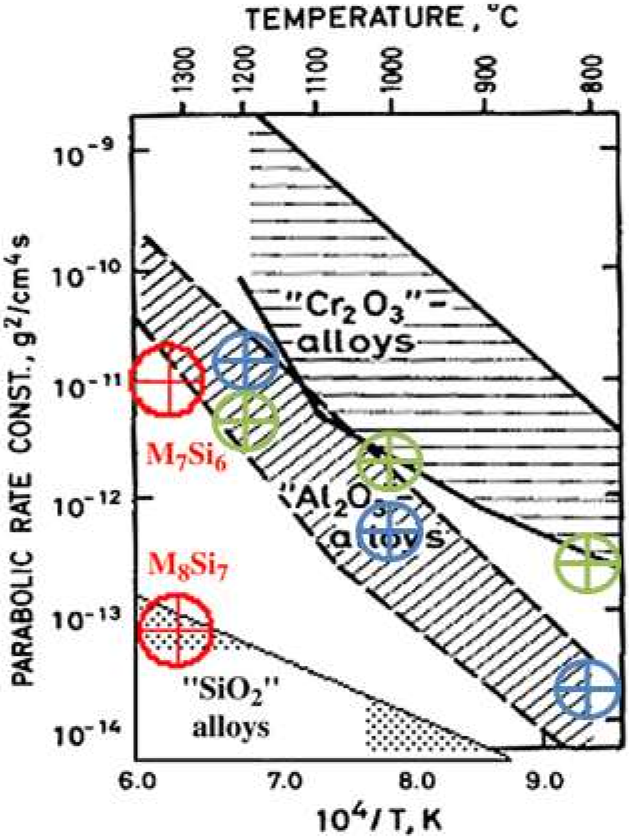

Figure 6.28 kp value fields of chromia, silica and alumina-forming alloys, the oxidation rates of alloy AN3 and AN4 are pointed by blue and green cross respectively. Red cross is oxidation rate of silicides studied by Zamoum et al. [103,129].

A summary of the scales formed on the alloy AN3 and AN4 is given in Table 6-6. The morphology of the scale changed from whiskers to cells to ridges or buckled scales with the exception of the alloy AN3 at 1200 ^{o}C which had a smooth scale without any corrugation. At 1200 ^{o}C, the alloy AN3 suffered from scale spallation due to thermal expansion mismatch between the alumina and substrate or due to the formation of interfacial voids. The scales grown on the alloy AN4 developed a convoluted morphology at 1200 ^{o}C. The lateral growth in oxide scale is indicated by scale buckling. Lateral growth of oxide can occur by lattice diffusion of appropriate anion and cation point defects and/or by grain boundary diffusion of one or both metal and oxygen as reactants. Transport of reactants in alumina scales, however, is not well understood; diffusion and marker measurements indicate that alumina layers grow inward by oxygen transport occurring predominantly at grain boundaries, and a lesser but significant flux of Al diffusing through the lattice. Oxide formation at grain boundaries would give rise to compressive stress in the oxide and a residual tensile stress in the oxide exceeds a critical value, which depends on the ability of the oxide to relief the stress and energy required to produce a new surface. The oxide when separated from the alloy either because of void formation or massive separation by buckling is observed to thicken and grow laterally, this necessities a mode of Al transport from the alloy surface to the underside of the detached scale [139].

6.4. Summary

I. The phases present in the as-cast and heat treated alloy AN3 were the orthorhombic V_6Si_5-type Ti_6Si_5, the tetragonal W_5Si_3-type Cr_5Si_3, the hexagonal $CrSi_2$-type $CrSi_2$ and cubic CrSi- type CrSi (present only in the alloy heat treated at 1300°C) whereas the Ti_6Si_5, cubic Cr_3Si-type Cr_3Si , tetragonal Cr_5Si_3 and hexagonal Ti_5Si_3 silicide together with the rhombohedral Cr_5Al_8–type Cr_5Al_8, cubic Cu_5Zn_8-type Cr_4Al_9 and triclinic Mn_4Al_9–type $Cr_{11}Al_4$ were formed in the alloy AN4 (the $Cr_{11}Al_4$ was only present after the heat treatment at 1300 °C).

II. The suggested solidification path for AN4 is $L \rightarrow L+T \rightarrow L+T+T1 \rightarrow L+T+T1+Cr_5Al_8 \rightarrow T+T1+Cr_5Al_8+Cr_4Al_9$.

III. The T phase $(Ti,Cr)_6Si_5$ is stabilised by the synergy of Cr and Ti with Al and Si, and Al controls the stability of CrSi and $CrSi_2$ which it suppresses in favour of Cr_3S, particularly when its concentration in the alloy is high enough to lead to the formation of stable aluminide(s) with C. Titanium plays a key role as the microstructure approaches equilibrium.

IV. The alloy AN3 formed a composite scale consisting of alumina, mullite and chromia with good adhesion to the substrate at 800 and 1000 °C. At 1200 °C a continuous alumina scale formed but had a poor adhesion to the substrate and spalled off.

V. The alloy AN4 formed a composite scale at 800 °C, consisting of alumina, mullite and chromia with good adhesion to the substrate. Alumina formed on the surface of the alloy at 1000 and 1200 °C. The scale was not fully adherent to the substrate at 1000 °C and partially spalled.

VI. The alloys AN3 and AN4 followed parabolic/near parabolic oxidation in the temperature range 800 to 1200 °C, with the exception of alloy AN3 that exhibited paralinear oxidation at longer exposure time ($t>16$ h) at 1200 °C.

VII. The oxidation rate constants of the alloys AN3 and AN4 were comparable to those of Fe, Ni and Pt-based alloys at 1200 °C and at 800 to 1000 °C they were higher compared with Al rich intermetallics.

VIII. The activation energies for oxidation of AN3 and AN4 alloy were 90.3 and 32.4 kJ/mol respectively.

The evidence for alloys AN3 and AN4 would thus suggest that in the Al rich alloy AN4 with Ti addition the $CrSi_2$ is not stable while the Al_8Cr_5 is stable as well as $Al_{11}Cr_4$. The latter two phases are undesirable as they could lead to liquation in the microstructure at high temperatures according to the Al-Cr binary. Furthermore, the data for AN3 shows that with Ti as quaternary addition it is possible to form alumina in the scale up to 1200 ^{o}C without having a high concentration of Al in the alloy and achieve oxidation rate constant that are comparable to those of Ni and Pt based intermetallic alloys. The addition of Ti does reduce the solubility of Al in $CrSi_2$ more than Hf does, but this phase was not destabilized by the quaternary addition of Ti in the alloy AN3 (low Al content) and is believed to play a key role in the formation of alumina scale owing to its volume fraction in the Al poor alloy AN3 which is slightly higher than in AN1. The microstructure of alloy AN3 is also desirable because the intermetallics in the Cr-Si system are expected to be exhibiting good oxidation behaviour up to about 1200 ^{o}C [130] compared with Al-Cr intermetallics which are expected to have good oxidation behaviour up to but not exceeding 1000 ^{o}C and the densities of $CrSi_2$ and Cr_5Si_3 are desirable as they are about 5 and 6.5 g/cm^3 respectively [131,132]. (the density of Cr_3Si is 6.54 g/cm^3 [131] and this phase formed in AN2 but was not stable at 1300 ^{o}C). However with the addition of Ti in the Al poor alloy AN3 the CrSi was stabilised at 1300 ^{o}C but at very low volume fraction. This intermetallic has negligible solubility for Al.